Information Processing in Agriculture xxx (xxxx) xxx

Contents lists available at ScienceDirect

Information Processing in Agriculture

journal homepage: www.keaipublishing.com/en/journals/information-processing-in-agriculture/

Identification and reconstruction of grid-distributed wires in dense kiwifruit canopies based on geometric feature grouping-connection for robotic harvesting

Xiaojuan Liu [a], Bryan Gilbert Murengami [a], Qilin Gong [a], Xiaoyu Ma [a], Rui Li [a,*], Xiancun Zhou [b], Bao Zhou [b], Jinyong Chen [e], Ramesh Kumar Sahni [f], Yaqoob Majeed [g], Spyros Fountas [h], Longsheng Fu [a,b,c,d,*]

[a] College of Mechanical and Electronic Engineering, Northwest A&F University, Yangling, Shaanxi 712100, China
[b] School of Electronic Information and Artificial Intelligence, West Anhui University, Lu'an, Anhui 237012, China
[c] Shaanxi Key Laboratory of Agricultural Information Perception and Intelligent Service, Yangling, Shaanxi 712100, China
[d] Key Laboratory of Agricultural Internet of Things, Ministry of Agriculture and Rural Affairs, Yangling, Shaanxi 712100, China
[e] Zhengzhou Fruit Research Institute, Chinese Academy of Agricultural Sciences, Zhengzhou, Henan 450009, China
[f] Agricultural Mechanization Division, ICAR-Central Institute of Agricultural Engineering, Bhopal 462038, Madhya Pradesh, India
[g] Department of Electrical Engineering and Computer Science, University of Wyoming, Laramie, Wyoming 82071, United States
[h] Agricultural University of Athens, Athens 11855, Greece

ARTICLE INFO

Keywords:
Grid-distributed wires
Geometric feature analysis
Feature identification and extraction
Wire reconstruction
Robotic harvesting

ABSTRACT

Grid-distributed wires in T-trellis kiwifruit orchards provide structural support for dense canopy growth and enable mechanized operations such as robotic harvesting. However, these wires also introduce potential risks of collision and damage to the robot end-effector, particularly when target fruits are partially occluded by thin and visually inconspicuous wire structures. Therefore, accurate identification of wire segments and reconstruction of wire layouts are essential for safe and efficient robotic picking strategies. In this study, an identification and reconstruction method for grid-distributed wires in dense kiwifruit canopies was presented based on Geometric Feature Grouping-connection (GFG). First, fragmented wire segments were extracted from canopy images using a YOLO11x-seg model combined with an Image Overlap-partitioning and Stitching (IOS) strategy. Then, the proposed GFG approach grouped and connected discrete wire segments through directional classification, spatial grouping, and boundary extension, enabling complete reconstruction of grid-distributed wire structures. Experimental results show that the model trained on the overlap-partitioned dataset achieved an average precision of 28.50% at an Intersection over Union (*IoU*) threshold of 0.5, representing a 13.50% improvement over the model trained on the original dataset. With the integration of IOS strategy, the model achieved an *IoU* of 21.19% and a Pixel Accuracy (*PA*) of 21.00%, corresponding to improvements of 9.54% and 10.00%, respectively, compared with the baseline without IOS. In addition, the proposed GFG approach achieved a reconstruction accuracy of 78.28% for grid-distributed wire structures. Overall, these findings indicate that the presented method enables the reliable identification of fragmented wire segments and reconstruction of continuous grid-distributed wire structures in dense canopy environments. This study highlights the importance of reconstructing non-target support structures for improving orchard scene understanding and providing useful geometric information for future obstacle-aware robotic harvesting.

1. Introduction

Grid-distributed wires provide stable support for dense kiwifruit canopies and facilitate robotic harvesting. In China, kiwifruit orchards typically adopt low-cost T-bar trellis cultivation system where grid-arranged wires serve as the primary support structure [1,2]. These grid wires are spaced 50 cm apart parallel to the tree rows and 3.5 m apart perpendicular to the rows [3]. This arrangement creates a

* Corresponding author at: College of Mechanical and Electronic Engineering, Northwest A&F University, Yangling, Shaanxi 712100, China.
E-mail addresses: ruili1216@nwafu.edu.cn (R. Li), fulsh@nwafu.edu.cn (L. Fu).

https://doi.org/10.1016/j.inpa.2026.07.007
Received 29 November 2025; Received in revised form 2 July 2026; Accepted 23 July 2026
Available online 27 July 2026
2214-3173/© 2026 Published by Elsevier B.V. on behalf of China Agricultural University. This is an open access article under the CC BY-NC-ND license (http://creativecommons.org/licenses/by-nc-nd/4.0/).

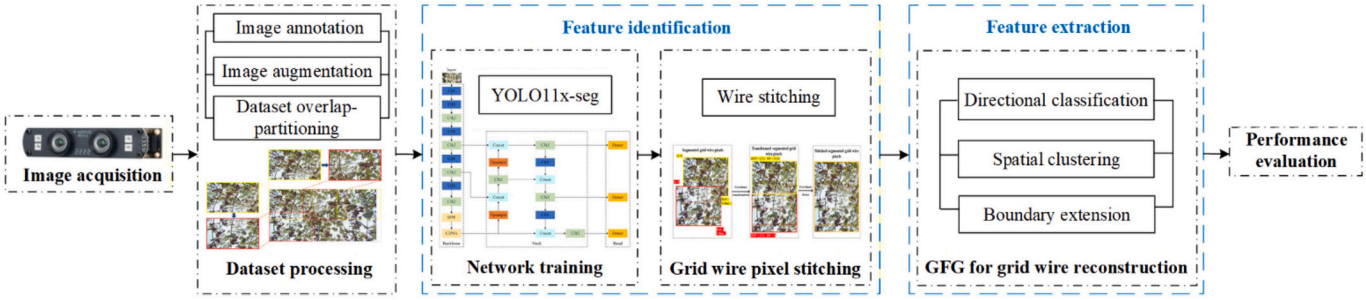


Fig. 1. Overview of the overall workflow in this work.

structured three-dimensional spatial architecture that improves light transmission and helps maintain canopy integrity. Compared to unstructured orchards, the grid-based layout enhances fruit visibility by optimizing the spatial distribution of branches and fruit locations [4]. Moreover, the organized wire architecture establishes a clear geometric reference framework. Accurate reconstruction of this framework is crucial for developing reliable obstacle avoidance and motion planning strategies in automated harvesting, as it can simplify the path search space for end-effectors. From the perspective of data-driven smart agriculture, such reconstructed canopy structure information can also serve as field level perception data for IoT-assisted orchard monitoring and management [5].

Accurate and robust identification of wires beneath dense canopies is critical for enabling efficient robot harvesting. In kiwifruit orchard images, target fruits are often intermixed with non-target obstacles such as leaves, branches, and support wires, making reliable scene understanding and obstacle discrimination particularly challenging [6,7]. Most existing studies primarily focus on identifying target fruits, including fruits that are adjacent, clustered, or occluded, while neglecting non-target obstacles that can significantly affect fruit detection accuracy and harvesting performance [8–10]. Effective identification of these non-target obstacles is essential for optimizing harvesting strategies and improving overall picking efficiency [11]. Among these obstacles, support wires pose a significant risk to robotic harvesting end-effectors, potentially causing mechanical damage operational interruptions, and reduced harvesting efficiency [3,9,12]. Consequently, accurate identification of wires within the robot's operational workspace is critical for ensuring safe, reliable, and efficient robotic harvesting. In practical smart-orchard deployment, high-resolution canopy perception data also need to be efficiently processed at the edge and securely transmitted and stored within agricultural IoT systems.

Deep learning algorithms have been extensively applied to identify key target information from orchard imagery. For example, Williams et al. [13] utilized Faster-RCNN for real-time fruit detection under real-world lighting conditions, achieving a detection rate of 90.7%. Kok et al. [14] used Wire-CLRNet for trellis wire detection in occluded outdoor conditions, obtaining an mF_1 score of 0.9345. Currently, the Ultralytics's YOLO (You Only Look Once) series models, along with their various modified variants, have been extensively applied due to their strong balance among detection accuracy, computational efficiency, real-time performance, and lightweight deployment capabilities [15–24]. Meanwhile, a comprehensive evaluation of the YOLO series in complex orchard environments was reported in [25], providing practical insights for selecting suitable YOLO11 variants for fruitlet detection under field conditions. Therefore, employing an advanced instance segmentation network is both effective and necessary for accurate identification and segmentation of support wires within dense kiwifruit canopies.

Wire segmentation presents a unique challenge due to the thin structural characteristics of wires and their frequent occlusion by fruits, branches, leaves, and varying illumination conditions within orchard environments. For instance, Jiang et al. [11] proposed an image overlap-partitioning and stitching (IOS) algorithm for BlendMask to segment wires in apple orchards. Their approach achieved an average precision of 38.75% at an IoU (Intersection over Union) threshold of 0.5 on overlap-partitioned datasets, representing a 38.42% improvement compared to full-image training strategies. Majeed et al. [26] applied SegNet to segment trunks, branches, and wires in both simple-RGB and foreground-RGB apple orchard images, reporting IoU values of 0.61, 0.46, and 0.29, respectively. Similarly, Kok et al. [14] developed Wire-CLRNet and achieved an IoU of 0.88 for apple trellis wire segmentation under occluded outdoor conditions. Moreover, Song et al. [3] employed DeepLabV3+ with uniform weights to segment calyxes, branches, and wires in kiwifruit images, achieving IoUs of 0.68, 0.70, and 0.42, respectively. However, most existing studies have been conducted in orchards with relatively simple canopy structures and regular spatial arrangements.

Although these methods demonstrate promising performance, they largely focus on wire reconstruction in constrained and controlled scenarios. These studies provide limited investigation into more complex and diverse orchard environments or into how reconstructed wire information can effectively guide robotic end-effectors during harvesting operations [3,11,14]. Additionally, comparative analysis indicate that wires consistently yields lower IoU than other targets, primarily due to the extremely limited proportion of representative wire pixels and severe occlusion effects, both of which negatively impact segmentation robustness and operational accuracy [3,11,14,26]. Therefore, further research on robust wire reconstruction under dense and highly occluded canopies is needed to support safer, reliable, and efficient robotic harvesting systems. In particular, increasing the representation of wire pixels within training datasets is a practical and important strategy for improving model robustness, wire detection accuracy, and the overall effectiveness of wire reconstruction and robotic harvesting operations.

Based on the aforementioned research gaps, this paper presents a novel method for identifying and reconstructing grid-distributed wires in dense kiwifruit canopies. First, wire images are captured using an upward-facing imaging configuration positioned beneath kiwifruit canopy to acquire complex orchard scenes. Next, fragmented wire segments are extracted from canopy images and recovered into full-resolution wire structures. Finally, the central contribution of this work lies in the proposed Geometric Feature Grouping-Connection (GFG) approach, which converts fragmented wire segments extracted from dense canopy images into continuous grid-distributed wire structures. Unlike studies that focus mainly on wire segmentation, the GFG approach reconstructs the geometric layout of support wires through a three-stage processing pipeline, including directional classification, spatial clustering, and boundary extension. In this framework, YOLO11x-seg with IOS is adopted to improve the extraction of fragmented wire segments, whereas GFG serves as the core reconstruction module that provides structured geometric information for obstacle awareness in robotic harvesting. The remainder of this paper is organized as follows: Section 2 describes the materials and methods, including image acquisition, image processing, network architecture and training procedures, the wire reconstruction methodology. Section 3 presents experimental results along with detailed discussion and

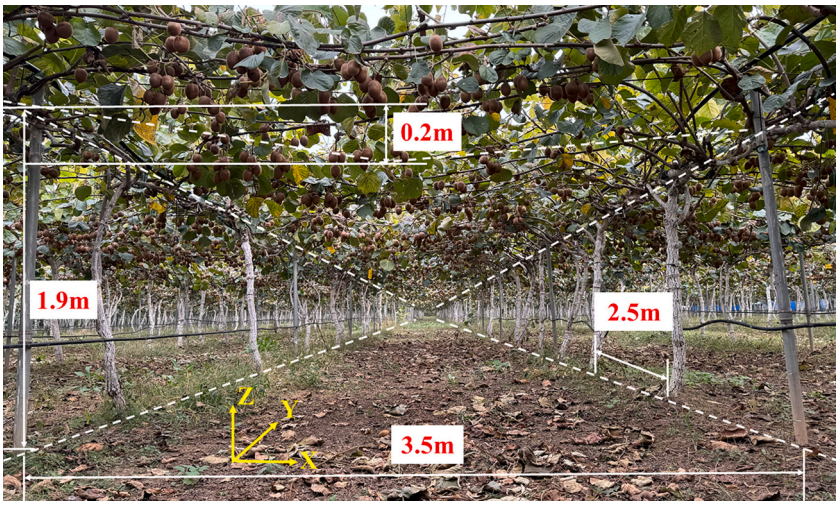


Fig. 2. Kiwifruit orchard environment and planting parameters.

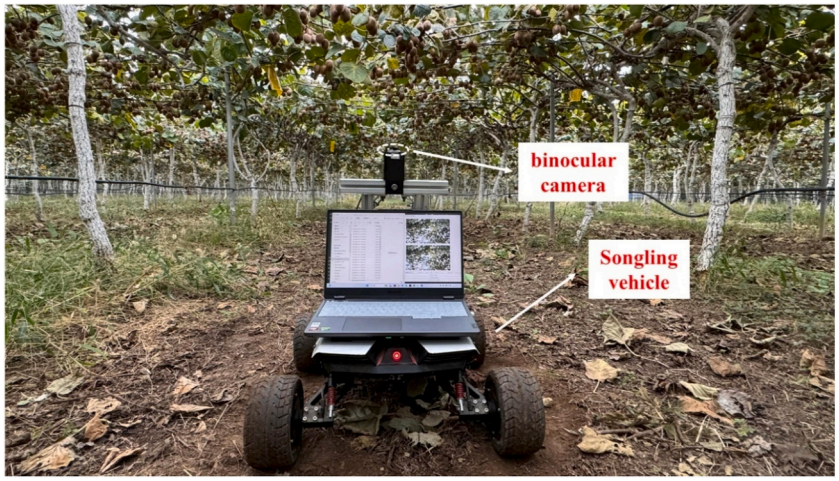


Fig. 3. Image acquisition system in orchards. The system consists of a Songling vehicle equipped with a binocular camera, mounted on a 3D-printed adapter secured to a custom-designed aluminum frame positioned.

analysis. Finally, Section 4 summarizes the conclusions and future research directions.

2. Materials and methods

This study focuses on the identification and reconstruction of grid-distributed wires within dense kiwifruit canopies through an integrated framework combining wire segmentation and reconstruction methods. The overall workflow and specific processing pipeline of the proposed approach is illustrated in Fig. 1, while the detailed methodology and implementation procedures are described in the following sections.

2.1. Image acquisition

Experimental RGB (Red, Green, and Blue) images were collected from Aiqiyi farm (Orchard-1, latitude: 34°20′N, longitude: 108°19′E, and average altitude: ~430 m) and Lvyilong orchard (Orchard-2, latitude: 34°33′N, longitude: 108°11′E, and average altitude: ~514 m) in Wugong County, Shaanxi Province, China, during September and November 2024. Orchard-1 images were acquired under cloudy weather conditions, while Orchard-2 images were captured under sunny conditions with relatively dense canopies coverage. As illustrated in Fig. 2, orchard employs grid-wire trellis cultivation system to regulate kiwifruit canopy growth and spatial structure. Key planting parameters include a plant spacing of 2.5 m, row spacing of 3.5 m, canopy height of 1.9 m, and a vertical fruit distribution variation of 0.2 m. This standardized cultivation system facilitates consistent orchard management and provides a controlled experimental environment for evaluating mechanize agricultural operations [27,28].

Image acquisition was performed using a Songling vehicle equipped with a binocular camera system (Jieruiweitong, Shenzhen, China) operating at a resolution of 2560 × 1440 pixels. The imaging system was mounted on a 3D-printed adapter fixed to a custom-designed aluminum frame, positioned approximately 60 cm above ground level and oriented vertically upward to capture canopy structure (Fig. 3). The camera provides a wide field of view (diagonal angle: 100°, horizontal angle: 85°), enabling comprehensive coverage of the canopy architecture within a single frame. RGB images were recorded in 'JPG' format under natural daylight conditions with varying illumination levels to ensure dataset diversity and robustness.

2.2. Image annotation and augmentation

A total of 142 RGB images were collected to construct the original dataset. All images were manually annotated at the pixel level using

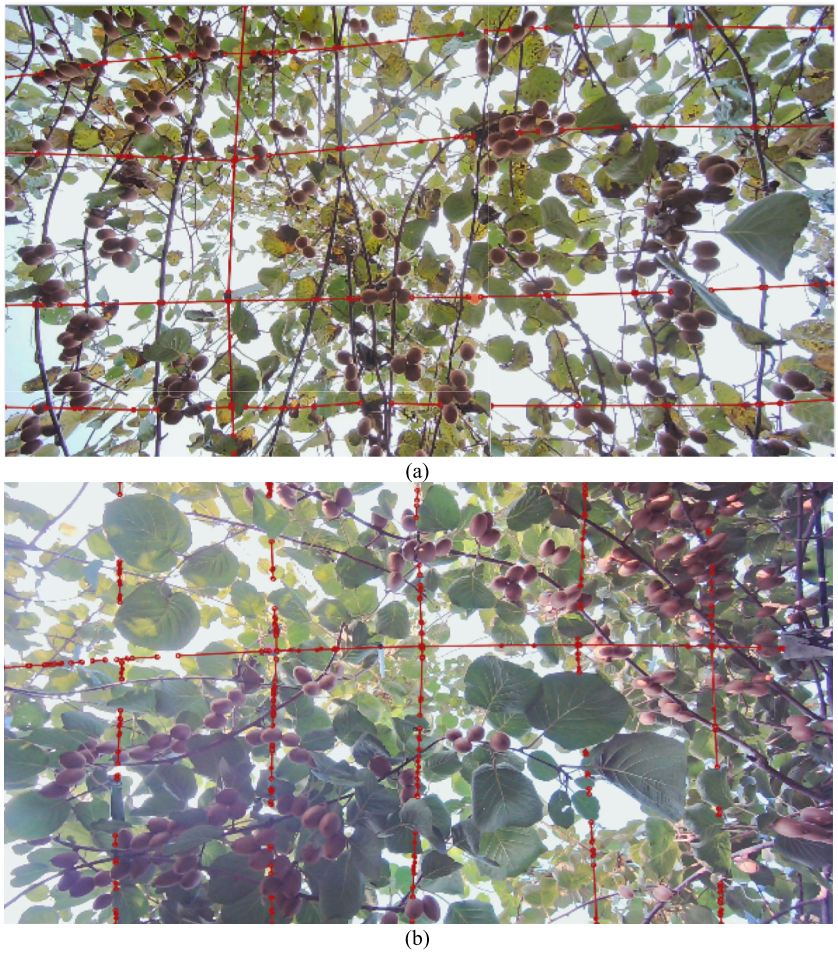


Fig. 4. Representative examples of annotated grid-distributed wires beneath kiwifruit canopies in RGB images. Wire annotations are shown in (a) Orchard-1 and (b) Orchard-2, where red polygons indicate annotated wire regions. (For interpretation of the references to colour in this figure legend, the reader is referred to the web version of this article.)

Labelme [29], developed by the Computer Science and Artificial Intelligence Laboratory, MIT. Fragmented wire segments were manually annotated as polygons with the class name 'wire'. After annotation, each image was exported and stored in 'JSON' format. Representative examples of annotated grid-distributed wires beneath kiwifruit canopies are shown in Fig. 4. The dataset was randomly split into a training set (99 images) and testing set (43 images), corresponding to a ratio of 7 to 3.

Given the limited representation of wire pixels and the inherent challenges in training a robust deep learning model, data augmentation techniques were applied to enhance dataset diversity and improve model generalization [30]. A total of thirteen augmentation strategies were employed, including brightness adjustment, contrast variation, chroma transformation, sharpness modification, and blurring operations (Gaussian and smoothing). The transformation parameters were set with brightness, contrast, and chroma factors of 0.7, 0.9, and 1.3, respectively. Following augmentation, the original training set was expanded from 99 images to 1287 images. The train-test split was conducted at the original-image level before data augmentation and overlap partitioning, ensuring that augmented samples and overlap-partitioned sub-images from the same original image were kept within the same subset. This prevented direct sample leakage between the training and testing sets. However, since the images were collected from two orchards with similar T-trellis cultivation structures and a consistent upward-facing imaging configuration, the current evaluation is a within-orchard evaluation rather than a strict orchard-independent validation, and the reported performance may be slightly optimistic for completely unseen orchard environments.

2.3. Dataset overlap-partitioning

Unlike other target objects in dense kiwifruit canopies, grid-distributed wires are extremely slender, making their pixel representation sparse and posing significant challenges for pixel-level wire segment extraction. To increase the proportion of wire pixels in the training data and improve feature learning, the original images were further processed using an overlap-partitioning strategy following the methodology of Jiang et al. [11]. Using Orchard-1 as an example, each original image was partitioned into overlapping sub-images, as illustrated in Fig. 5. Specifically, each image of resolution 2560 × 1440 pixels was divided into six sub-images of 1024 × 800 pixels in a top-left to bottom-right scanning order, with a 20% overlap between adjacent regions to preserve contextual continuity. Regions outside the image boundaries in the last row or column were padded with a green background to maintain consistent input dimensions. After partitioning, the dataset was expanded to a total of 852 images, including 594 training samples. The corresponding annotation masks were partitioned using the same overlap strategy to ensure strict pixel-level alignment between images and labels.

2.4. Network architecture and training

Single-stage and two-stage visual recognition models were comparatively analyzed to provide reliable wire segments for subsequent GFG-

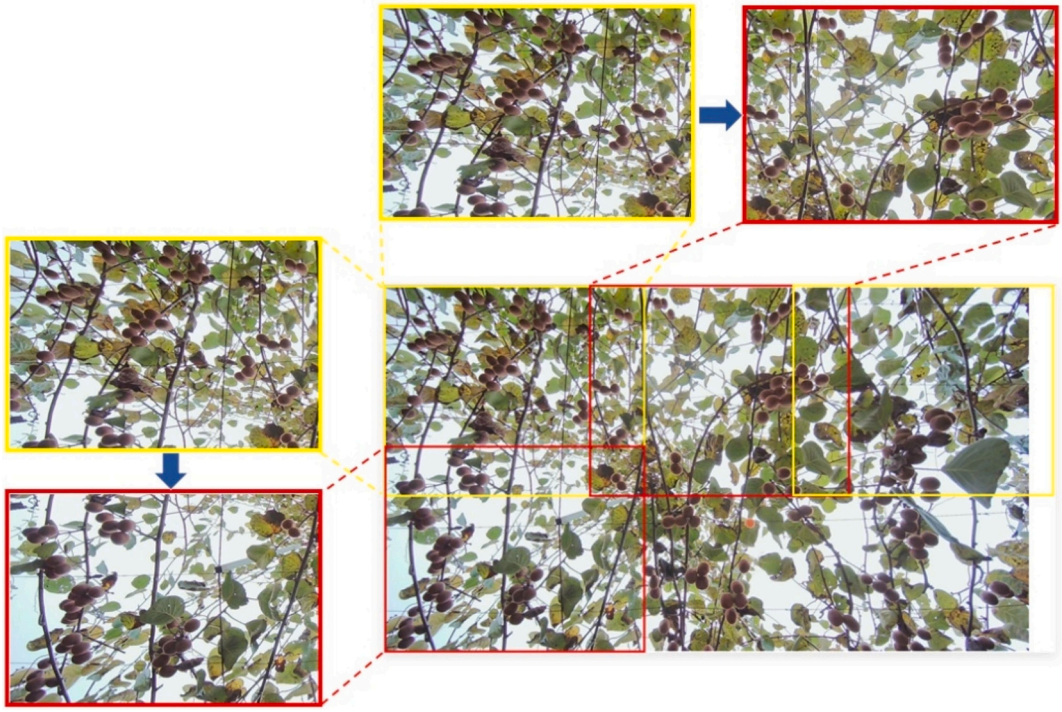


Fig. 5. Example of overlap-partitioning of an original image from Orchard-1, organized into a grid corresponding to the rows and columns of the original image. Sub-images with yellow borders overlap with adjacent images outlined in red by 20%. (For interpretation of the references to colour in this figure legend, the reader is referred to the web version of this article.)

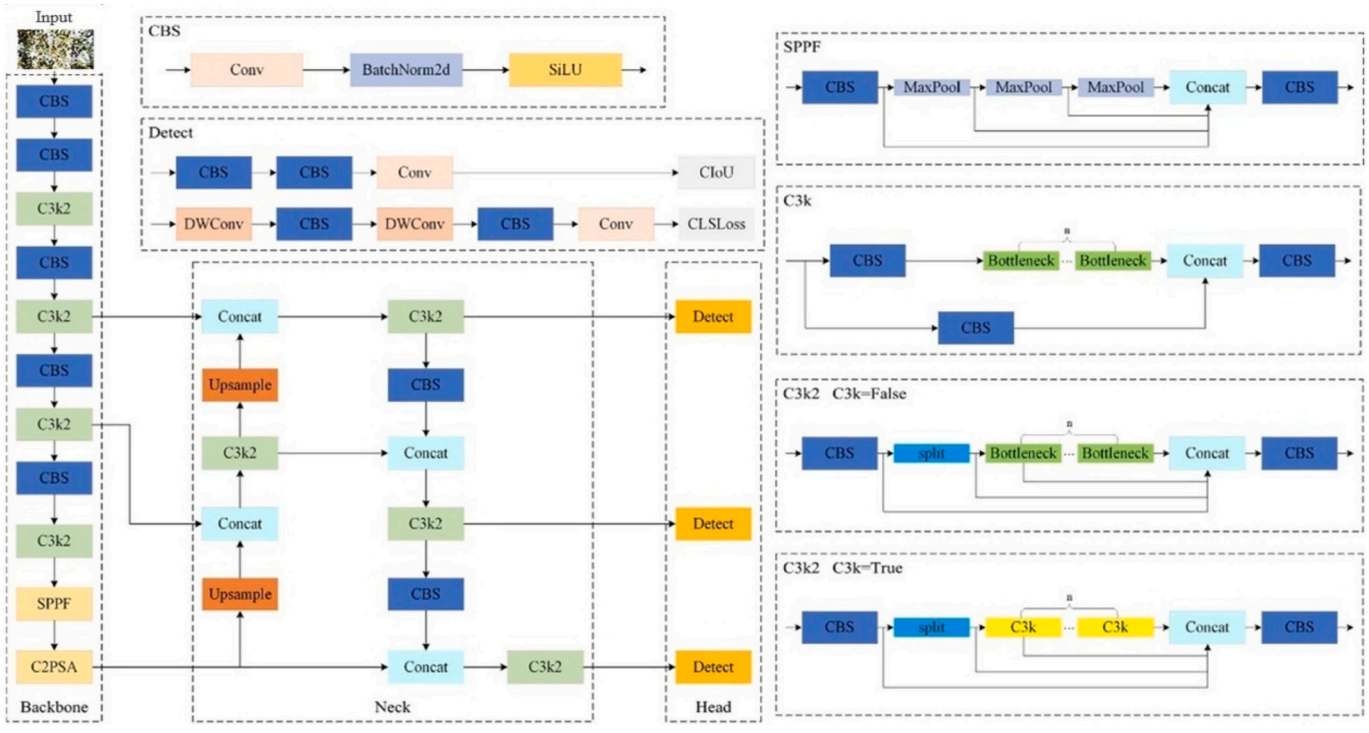


Fig. 6. Network architecture of YOLO11 [20].

based wire reconstruction. Two-stage frameworks, such as Faster R-CNN and Mask R-CNN, first generate region proposals followed by classification and segmentation, which can provide high detection accuracy but introduces substantial computational latency due to their serial processing pipeline. In contrast, single-stage models, such as Ultralytics YOLO series, perform detection and segmentation through a unified forward-pas architecture, enabling an optimal balance between inference speed and detection accuracy [31]. This end-to-end design is particularly suitable for real-time orchard perception applications and aligns well with the operational requirements of this study. Among the YOLO series, YOLO11 provides a robust foundation for instance segmentation tasks in smart agriculture due to its well-established

Table 1
Training parameters of YOLO11x-seg.

Training parameters	Values
Backbone	Variant of CSPDarknet53
Pre-trained weight initialization	YOLO11x-seg
Input resolution	1280 × 1280
Batch size	1
Training epoch	300
Learning rate	0.002
Momentum	0.9
Warmup epochs	3.0
Warmup_momentum	0.8
Weight decay	0.0005
Patience	50
Weight optimizer	Adam with Decoupled Weight Decay (AadmW)

architecture and deployment stability [32]. Based on these advantages, YOLO11x-seg was selected as the baseline model because of its higher segmentation performance.

YOLO11 has demonstrated remarkable accuracy, fast inference speed, and high computational efficiency for real-time object detection. Building upon the major advancements introduced in earlier YOLO versions, YOLO11 incorporates an enhanced backbone and neck architecture that significantly improves feature extraction capabilities and overall detection performance, making it highly suitable solution for a wide range of computer vision applications [32,33]. These capabilities are particularly advantageous for identifying thin and partially occluded grid-distributed wires within dense kiwifruit canopies. The YOLO11 network architecture consists of four components, i.e., Input, Backbone, Neck, and Head, as illustrated in Fig. 6 using the default network parameters.

Compared with YOLOv8, the YOLO11 architecture introduces several multidimensional enhancements aimed at improving feature representation, computational efficiency, and detection robustness. First, the C3k2 module replaces the earlier C2f structure, facilitating multi-scale feature fusion through convolution and splicing operations [20]. Second, a C2PSA module is introduced after the SPPF module, extending the C2F structure by incorporating PSA, which improves the network's ability to emphasize informative spatial and contextual features while improving overall feature representation [33]. Finally, the Detect module incorporates two depth-wise convolution operations into the original detection head, substantially reducing computational complexity and parameter size of the detection head [32,33]. These architectural improvements enhance feature interaction through modular optimization and provide synergistic gains in attention weight allocation, multi-scale context perception, and computational efficiency management [20,32,33].

All experiments were conducted within the PyTorch framework (version 1.10.2). Model training and evaluation were performed on a desktop computer configured with Intel (R) Xeon (R) Gold 5218 CPU and an NVIDIA RTX 4090 GPU, with 128 GB of RAM, operating under Windows 10 64-bit system. The software environment included CUDA 10.1, CUDNN 11.0, Python 3.10, and OpenCV 4.1. In this study, the selected model was employed for wire segmentation training under the PyTorch framework, and the corresponding training hyperparameters are shown in Table 1.

2.5. Grid wire pixel stitching

Wire segment extraction was performed on the overlap-partitioned images, resulting in fragmented and discrete wire predictions across multiple sub-images. Therefore, a stitching process was required to recover full-resolution wire structures corresponding to the original images. Following the stitching principle of the IOS algorithm proposed by [11], the same coordinate transformation and stitching strategy was adopted to merge wire segment pixels from adjacent sub-images. Fig. 7 illustrates the stitching process for segmented grid wire pixels between two adjacent overlap-partitioned images within the same column. Specifically, the transformed coordinates of segmented wire pixels were calculated based on their original coordinates prior to transformation. The detailed mathematical formulations for wire pixels stitching are described in Jiang et al. [11] and are therefore not repeated here.

2.6. Geometric feature grouping-connection for grid wire reconstruction

Extracted wire segments were used as the input for subsequent GFG-based reconstruction. For each detected wire instance, polygon vertices were transformed into image coordinate space and exported as standard 'JSON' files compatible with Labelme software, along with optional 'TXT' files and visualized outputs for result verification. These standardized geometric annotations provide structured representations of segmented wire regions and serve as direct inputs for the subsequent wire reconstruction.

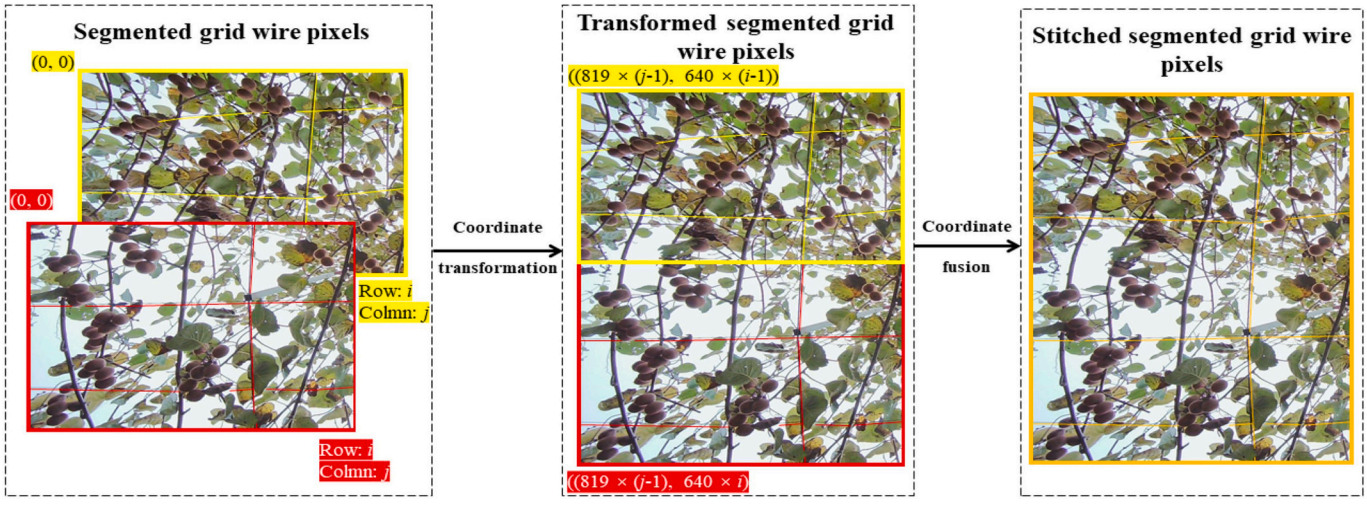


Fig. 7. Process of grid wire pixels stitching. (a) Segmented grid wire pixels from two adjacent overlap-partitioned images, highlighted with yellow and red lines; (b) Transformed segmented grid wire pixels; (c) Stitched segmented grid wire pixels, shown in orange lines. (For interpretation of the references to colour in this figure legend, the reader is referred to the web version of this article.)

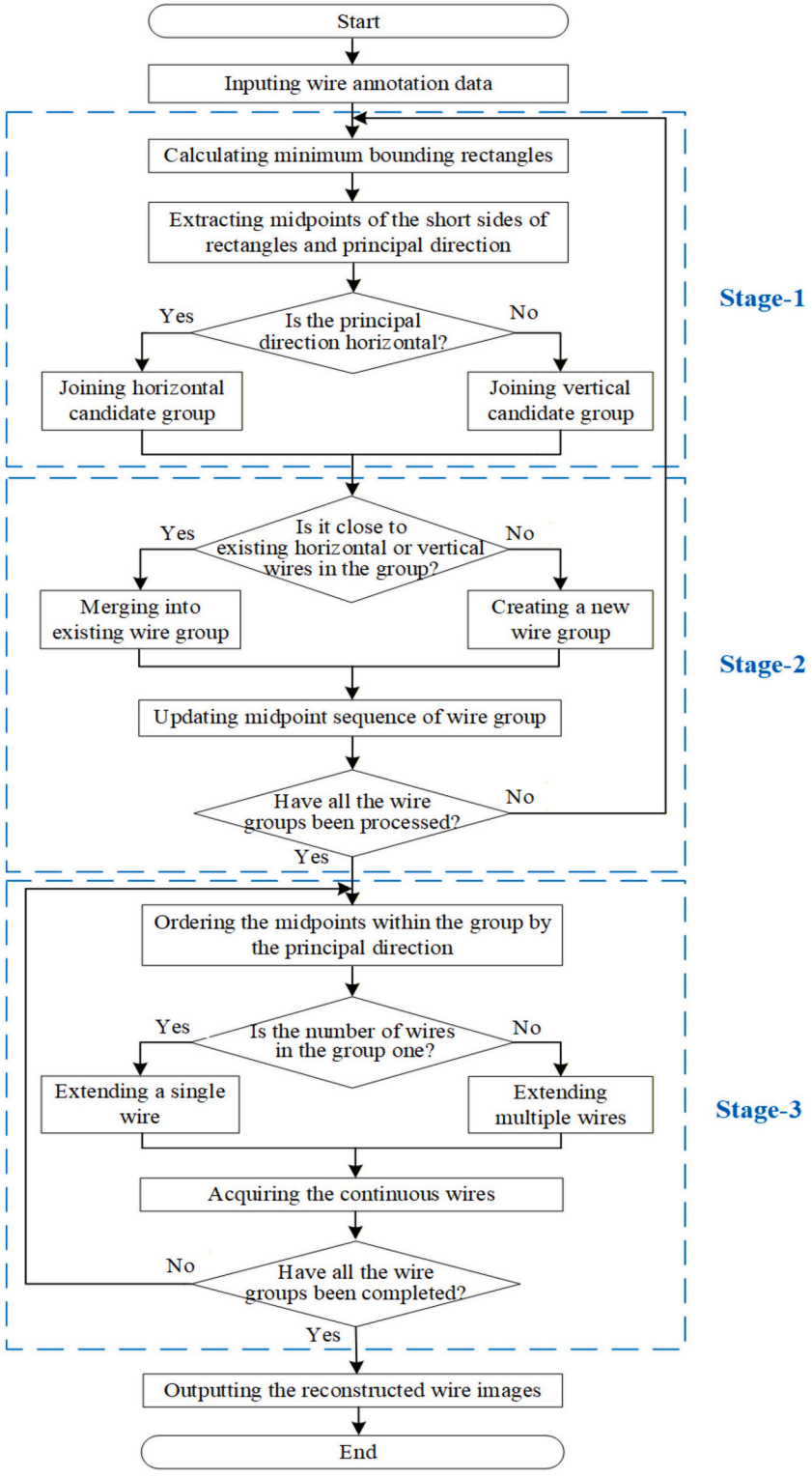


Fig. 8. Overall flowchart of GFG approach for grid wire reconstruction. It comprises directional classification (Stage-1), spatial clustering (Stage-2), and boundary extension (Stage-3).

Considering the agronomic characteristics of kiwifruit orchards, a Geometric Feature Grouping-Connection (GFG) approach was adopted for wire reconstruction. The proposed approach operates through a three-stage processing pipeline, consisting of directional classification (Stage-1), spatial clustering (Stage-2), and boundary extension (Stage-3). Segmented discrete wire segments were sequentially processed through these stages to progressively reconstruct complete and continuous grid-distributed wire structures within dense canopies. A schematic overview of the proposed GFG-based grid wire reconstruction process is illustrated in Fig. 8.

Stage-1: Directional classification. The spatial distribution of orchard wires provides the basis for directional classification and structural grouping, forming the foundation for preliminary wire reconstruction. Geometric features of each wire segment were extracted

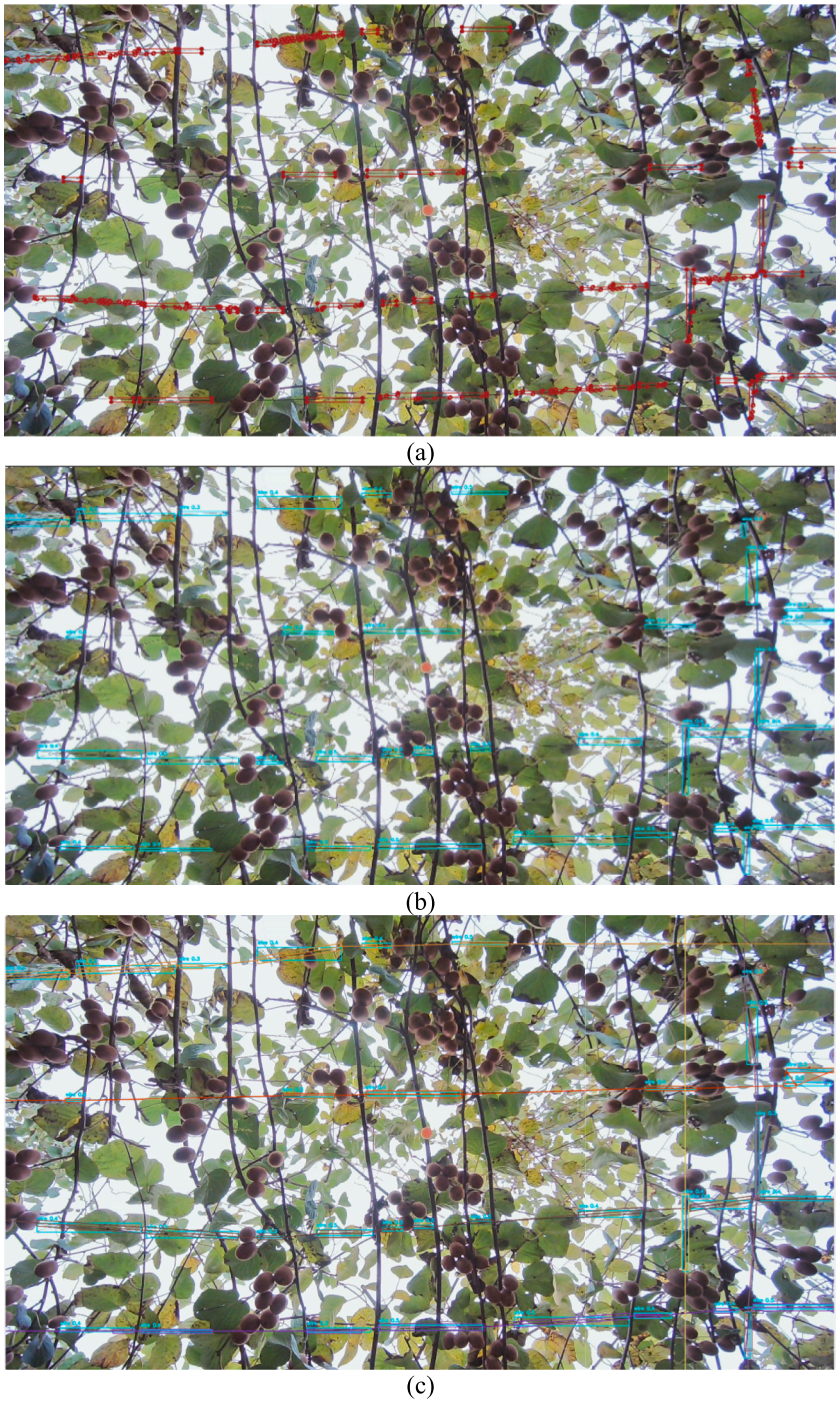


Fig. 9. Process of grid wire reconstruction using the proposed GFG approach. (a) Extracted wire pixel image from segmented (stitched) image by YOLO11x-seg with IOS; (b) Visualization of wire segment information corresponding to the extracted wire pixel image shown in 'a'; (c) Final reconstructed grid wire image corresponding to segmented (stitched) image.

by fitting a minimum bounding rectangle around the corresponding polygon region. To suppress segmentation noise and eliminate small fragmented regions, a size-based pre-filter criterion was applied, retaining only wire segments satisfying $\max(\Delta x_{\max}, \Delta y_{\max}) > \tau_s$, where τ_s was empirically set to 15 pixels. Here, $\Delta x_{\max}$ and $\Delta y_{\max}$ represent the maximum projection spans of a wire segment on the X-axis and Y-axis, respectively, as defined in Eq. (1) and Eq. (2), while P denotes the point set corresponding to the wire segment polygon. For the retained wire segments, the principal direction was determined by comparing projection along the coordinate axes, as described in Eq. (3). Where, MD, HD, and VD refer to the principal direction, horizontal direction, and vertical direction, respectively.

$$\Delta x_{\max} = \max_{p,q \in P} \left| x_p - x_q \right| \tag{1}$$

$$\Delta y_{\max} = \max_{p,q \in P} \left| y_p - y_q \right| \tag{2}$$

$$\mathrm{MD} = \begin{cases} \mathrm{HD} & \text{if } \Delta x_{\max} \geq \Delta y_{\max} \\ \mathrm{VD} & \text{otherwise} \end{cases} \tag{3}$$

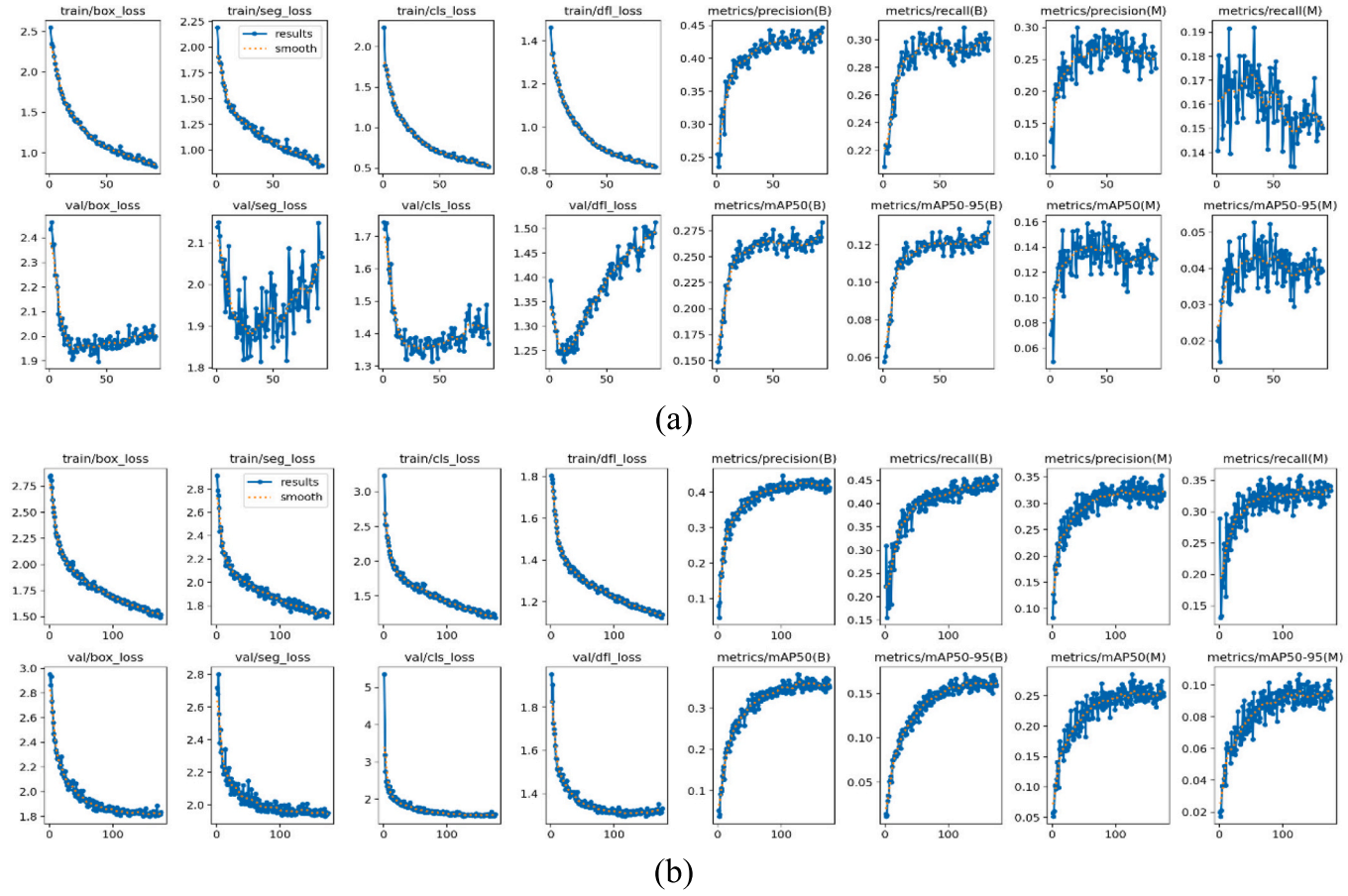


Fig. 10. Training loss curves of YOLO11x-seg trained on (a) original dataset and (b) overlap-partitioned dataset.

Table 2
Comparison of YOLO11x-seg models trained on original dataset and overlap-partitioned dataset.

Models	Dataset	*P*	*R*	*AP*	*AP*50
YOLO11x-seg	Original dataset	0.287	0.164	0.047	0.150
	Overlap-partitioned dataset	0.344	0.355	0.107	0.285

Stage-2: Spatial clustering. Based on the directional classification, wire segments sharing the same orientation were further clustered according to their spatial position. Specifically, wire segments with identical principal directions were aligned along the coordinate axes and grouped using a clustering threshold τ_c which was empirically set to 120 pixels. Horizontal wire groups were clustered based on differences in Y-axis coordinates, whereas vertical wire groups were clustered according to differences in X-axis coordinates, thereby forming direction-consistent candidate wire groups. The grouping criterion is defined in Eq. (4), where (X_i, Y_i) and (X_j, Y_j) represent the geometric center coordinates of two candidates wire segments, respectively. In addition, WG, HG, and VG denote the wire group, horizontal group, and vertical group, respectively, while τ_c represent the clustering threshold. Furthermore, the midpoints of the short sides of the fitted bounding rectangles were extracted for subsequent ordering and connectivity analysis, enabling reconstructing of fragmented wires segments along their principal directions.

$$\mathrm{WG} = \begin{cases} \mathrm{HG} & \text{if } |Y_i - Y_j| < \tau_c \\ \mathrm{VG} & \text{if } |X_i - X_j| < \tau_c \end{cases} \tag{4}$$

Two thresholds adopted in GFG have different functional roles. The size threshold τ_s was used to suppress small noisy fragments before directional classification, while the clustering threshold τ_c determined whether direction-consistent wire fragments should be grouped as the same wire structure. These values were empirically selected according to the image resolution, the observed scale of segmented wire fragments, and the regular spacing characteristics of grid-distributed wires in the T-trellis orchard system. A smaller τ_s may retain more noisy fragments, whereas a larger τ_s may remove short but valid wire segments. Similarly, a smaller τ_c may split fragments from the same wire into different groups, while a larger τ_c may incorrectly merge adjacent wires.

Table 3
Grid wire segmentation results of YOLO11x-seg with and without IOS.

Models	Adopted IOS	*IoU* (%)	*PA* (%)	Segmentation speed (ms/image)		
				Overlap-partitioning	Model Processing	Stitching
YOLO11x-seg	No	11.65	11.00	/	51.80	/
	Yes	21.19	21.00	290.00	174.80 × 6	117.20

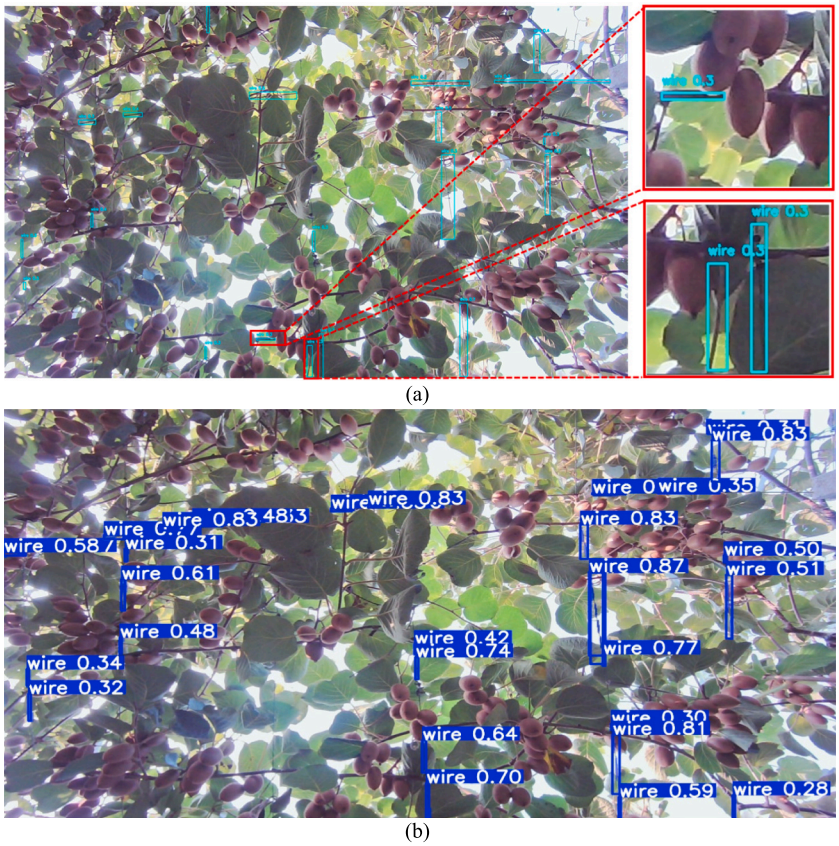


Fig. 11. Example of extracted segmented wire pixel results using YOLO11x-seg with IOS (a) and wire recognition and segmentation using YOLO11x-seg without IOS (b) for a grid canopy. Segmented wires in (a) are shown in sky blue, with minimum bounding rectangles displaying wire labels and confidence scores. Solid red rectangles denote manually annotated branches that were incorrectly segmented as wires. (For interpretation of the references to colour in this figure legend, the reader is referred to the web version of this article.)

Table 4
Evaluation of grid wire reconstruction using GFG approach.

Metrics	*RA* (%)	*MR* (%)	*IR* (%)	Reconstruction speed (ms/image)
Evaluation results	78.28	4.51	30.64	487

Therefore, these parameters are suitable for the tested kiwifruit T-trellis scenes but may require adjustment for orchards with different image resolutions, trellis spacing, or wire-curvature patterns.

Stage-3: Boundary extension. Within each clustered wire group, the midpoint sequences of wire segments were extended toward the image boundaries using slope estimation derived from midpoint pairs in the rectangles located nearest to the image edges. The resulting midpoint sets were subsequently ordered along the dominant axis and sequentially connected to reconstruct continuous wire structures. For groups containing only a single wire segment in the principal direction, the extension slope was directly obtained by extrapolating the line connecting the midpoints of the short sides of its bounding rectangle and extending it to the image boundary. For groups containing multiple wire segments, the extension direction was estimated using the slope of the line formed by the short-edge midpoints of two adjacent rectangles located closest to the image boundary, thereby ensuring smooth and consistent boundary transitions. The slope calculation for multiple wire segments is shown in Eq. (5), where (X_l, Y_l) and (X_r, Y_r) represent the short-edge midpoint coordinates of two adjacent rectangles closest to the image boundary. Finally, all obtained midpoints (including edge-extended points) were sorted according to the main direction and connected sequentially using line segments to reconstruct complete grid-distributed wire structures. The boundary extension is a constrained geometric completion based on the structural characteristics of grid-distributed wires in T-trellis kiwifruit orchards, rather than an arbitrary extension of fragmented wire segments. Therefore, the extended points represent inferred wire structures at the image level rather than directly observed wire pixels.

$$S = \frac{Y_r - Y_l}{X_r - X_l} \tag{5}$$

The entire reconstruction process strictly adheres to the principles of directional consistency and spatial distribution, enabling the transformation of discrete wire segments into complete and continuous grid-distributed wire structures. As illustrated in Fig. 9, the proposed GFG approach provides an intuitive and step-by-step visualization of grid wire reconstruction, demonstrating the effectiveness of each processing stage in recovering the structured wire geometry from fragmented segmentation outputs.

The pseudo-code of the GFG approach is provided in Algorithm 1.

Algorithm 1: GFG Pipeline for Grid Wire Reconstruction

Input: annotation set **A**, image I with width W and height H, size threshold $\tau_s = 15$ pixels, clustering threshold $\tau_c = 120$ pixels
Output: reconstructed image $I^{\bullet}$
$I^{\bullet} \leftarrow$ copy of I // initialize working copy
Step 1: Candidate Extraction and Directional Classification
$\mathbf{C} \leftarrow \emptyset$ // initialize candidate set
for each annotation $\mathbf{a} \in \mathbf{A}$ **do**
  $\mathbf{P} \leftarrow$ point set of $\mathbf{a}$ // extract polygon vertices
  if label of $\mathbf{a}$ starts with 'w' **then**
    compute $\Delta x_{max} \leftarrow \max_{\{\mathbf{p},\mathbf{q} \in \mathbf{P}\}} |x_p - x_q|$ and $\Delta y_{max} \leftarrow \max_{\{\mathbf{p},\mathbf{q} \in \mathbf{P}\}} |y_p - y_q|$
    if $\max(\Delta x_{max}, \Delta y_{max}) > \tau_s$ **then**
      if $\Delta x_{max} \geq \Delta y_{max}$ **then**
        $\mathbf{MD} \leftarrow \mathbf{HD}$ // set direction to horizontal
      else
        $\mathbf{MD} \leftarrow \mathbf{VD}$ // set direction to vertical
      end if
      store $(\mathbf{a}, \mathbf{P}, \mathbf{MD})$ in candidate set $\mathbf{C}$
    end if
  end if
end for
Step 2: Directional Spatial Clustering
$\mathbf{HG} \leftarrow \emptyset, \mathbf{VG} \leftarrow \emptyset$ // horizontal and vertical groups
for each candidate $\mathbf{c} \in \mathbf{C}$ **do**
  if $\mathbf{c.MD} = \mathbf{HD}$ **then** // check if candidate's principal direction is horizontal
    $\mathbf{G} \leftarrow \mathbf{HG}$ // assign to horizontal group
  else
    $\mathbf{G} \leftarrow \mathbf{VG}$ // assign to vertical group
  end if
  found $\leftarrow$ False
  for each group $\mathbf{g} \in \mathbf{G}$ **do**
    ref $\leftarrow$ first candidate of $\mathbf{g}$ // reference candidate
    if ($\mathbf{c.MD} = \mathbf{HD}$ and $\exists \mathbf{p} \in \mathbf{ref.P}, \exists \mathbf{q} \in \mathbf{c.P}$: $|y_p - y_q| < \tau_c$) or
      ($\mathbf{c.MD} = \mathbf{VD}$ and $\exists \mathbf{p} \in \mathbf{ref.P}, \exists \mathbf{q} \in \mathbf{c.P}$: $|x_p - x_q| < \tau_c$) **then**
      add $\mathbf{c}$ to group $\mathbf{g}$; found $\leftarrow$ True; **break**
    end if
  end for
  if found = False **then**
    create new group in $\mathbf{G}$ containing $\mathbf{c}$
  end if
end for
$\mathbf{WG} \leftarrow \mathbf{HG} \cup \mathbf{VG}$ // all non-empty groups
Step 3: Midpoint Extraction and Boundary Extension
for each group $\mathbf{g} \in \mathbf{WG}$ **do**
  $\mathbf{M} \leftarrow \emptyset, \mathbf{D} \leftarrow \emptyset$ // initialize midpoint set and direction votes
  for each candidate $\mathbf{c} \in \mathbf{g}$ **do**
    $\mathbf{B} \leftarrow$ minAreaRect($\mathbf{c.P}$) // compute minimum bounding rectangle
    extract short-edge midpoints $\mathbf{m_1}, \mathbf{m_2}$ and long-edge direction $\mathbf{d}$ from $\mathbf{B}$
    add $\mathbf{m_1}, \mathbf{m_2}$ to $\mathbf{M}$; add $\mathbf{d}$ to $\mathbf{D}$
    draw rectangle $\mathbf{B}$ on image $I^{\bullet}$
  end for
  $\mathbf{d_g} \leftarrow$ majority vote on $\mathbf{D}$ // determine principal direction of group
  if $|\mathbf{M}| = 2$ **then** // single wire segment
    compute slope $\mathbf{S}$ from $\mathbf{M}[1]$ to $\mathbf{M}[2]$ and extend to boundaries
    compute $\mathbf{m_left} = (0, y_0)$ and $\mathbf{m_right} = (W, y_1)$ using slope $\mathbf{S}$
    $\mathbf{M} \leftarrow [\mathbf{m_left}] \cup \mathbf{M} \cup [\mathbf{m_right}]$
  else // multiple wire segments ($|\mathbf{M}| > 2$)
    if $\mathbf{d_g} = \mathbf{HD}$ **then**
      sort $\mathbf{M}$ by $\mathbf{x}$-coordinate
      compute slopes $\mathbf{S_left}$ from $\mathbf{M[0]}$ to $\mathbf{M[1]}$ and $\mathbf{S_right}$ from $\mathbf{M[|M|-2]}$ to $\mathbf{M[|M|-1]}$
      compute $\mathbf{m_left} = (0, y_0)$ and $\mathbf{m_right} = (W, y_1)$ using $\mathbf{S_left}$ and $\mathbf{S_right}$
      $\mathbf{M} \leftarrow [\mathbf{m_left}] \cup \mathbf{M} \cup [\mathbf{m_right}]$
    else // vertical direction
      sort $\mathbf{M}$ by $\mathbf{y}$-coordinate
      compute slopes $\mathbf{S_top}$ from $\mathbf{M[0]}$ to $\mathbf{M[1]}$ and $\mathbf{S_bottom}$ from $\mathbf{M[|M|-2]}$ to $\mathbf{M[|M|-1]}$
      compute $\mathbf{m_top} = (x_0, 0)$ and $\mathbf{m_bottom} = (x_1, H)$ using $\mathbf{S_top}$ and $\mathbf{S_bottom}$
      $\mathbf{M} \leftarrow [\mathbf{m_top}] \cup \mathbf{M} \cup [\mathbf{m_bottom}]$
    end if
  end if
  for $\mathbf{i} \leftarrow 2$ to $|\mathbf{M}|$ **do**
    draw wire segments from $\mathbf{M[i-1]}$ to $\mathbf{M[i]}$ on $I^{\bullet}$
  end for
end for
return $I^{\bullet}$ // output reconstructed grid wire visualization

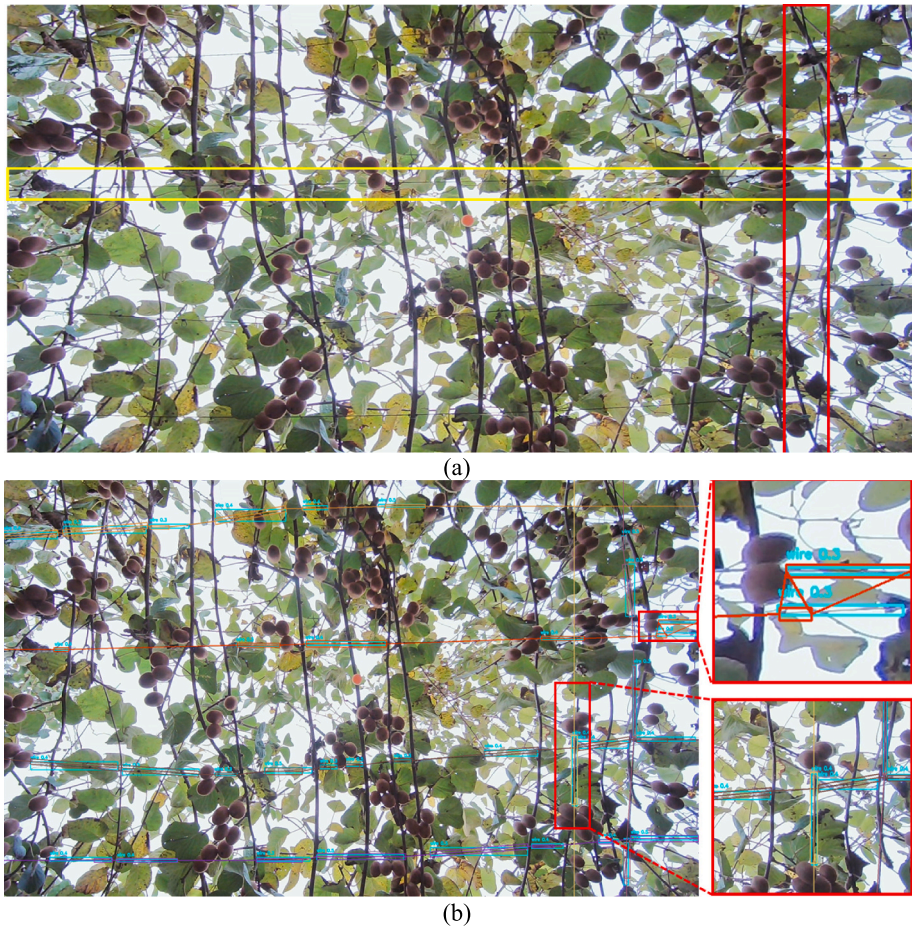


Fig. 12. Grid-distributed wire image (a) and its reconstruction effect (b) using the GFG approach. The yellow rectangle is one of horizontal wires, and the red rectangle is the vertical wire in (a). Distinctly colored lines represent the results of wire reconstruction in (b). Solid red rectangles indicate incorrect wire reconstructions, primarily caused by misidentified wire segments. (For interpretation of the references to colour in this figure legend, the reader is referred to the web version of this article.)

2.7. Performance evaluation

Performance of YOLO11x-seg was evaluated using Average Precision (*AP*) and Average Precision at an IoU threshold of 0.5 (*AP*50). Specifically, *AP* represents the mean precision computed over IoU thresholds ranging from 0.5 to 0.95 with a step size of 0.05, whereas *AP*50 corresponds to the average precision at IoU threshold of 0.5. Both *AP* and *AP*50 are derived from Precision (*P*) and Recall (*R*), as defined in Eq. (8) and Eq. (9), respectively. For the wire segmentation, a prediction is considered as True Positive (*TP*) when a wire instance is correctly detected. A False Negative (*FN*) occurs if wrongly detected and False Positive (*FP*) occurs when a wire is predicted but does not correspond to the ground truth label. Where, *P* is defined as the ratio of correctly detected wire instances to the total number of predicted wire instances, including both correct and incorrect ones, and *R* is defined as the ratio of correctly detected wire instances to the total number of actual ground truth instances, i.e., the sum of correctly wire instances and the number of ground truth that were not segmented.

$$P = \frac{TP}{TP + FP} \tag{6}$$

$$R = \frac{TP}{TP + FN} \tag{7}$$

$$AP = \left(\sum_{IoU=0.5}^{0.95} \int_0^1 P_{IoU}(R) dR \right) \Big/ 10 \tag{8}$$

$$AP50 = \int_0^1 P_{IoU=0.5}(R) dR \tag{9}$$

Performance of grid wire segmentation was evaluated using *IoU* and Pixel Accuracy (*PA*). *IoU* measures the proportion of overlapping region between predicted and ground truth wire pixels relative to their union area, as expressed in Eq. (10). *PA* evaluates the proportion of correctly classified pixels over the total number of pixels, as formulated in Eq. (11). In this formulation, the sum of ground truth wire pixels is represented by *A*, while the predicted wire pixels are represented by *B*, respectively. The *IoU* values ranges from 0.0 and 1.0. *K* represents the total number of categories (including background), and p_{ij} denotes the number of pixels of class *i* in ground truth images predicted as class *j* on segmented images, respectively.

$$IoU = \frac{|A \cap B|}{|A \cup B|} \tag{10}$$

$$PA = \frac{\sum_{i=0}^{K} P_{ij}}{\sum_{i=0}^{K} \sum_{j=0}^{K} P_{ij}} \tag{11}$$

Three metrics were used to evaluate the performance of grid wire reconstruction in the testing set: Reconstruction Accuracy (*RA*), Missed Rate (*MR*), and Incorrect Rate (*IR*). Specifically, *RA* represents the percentage of correctly reconstructed wires relative to the actual number of wires (i.e., the number of complete wires actually visible in the image).

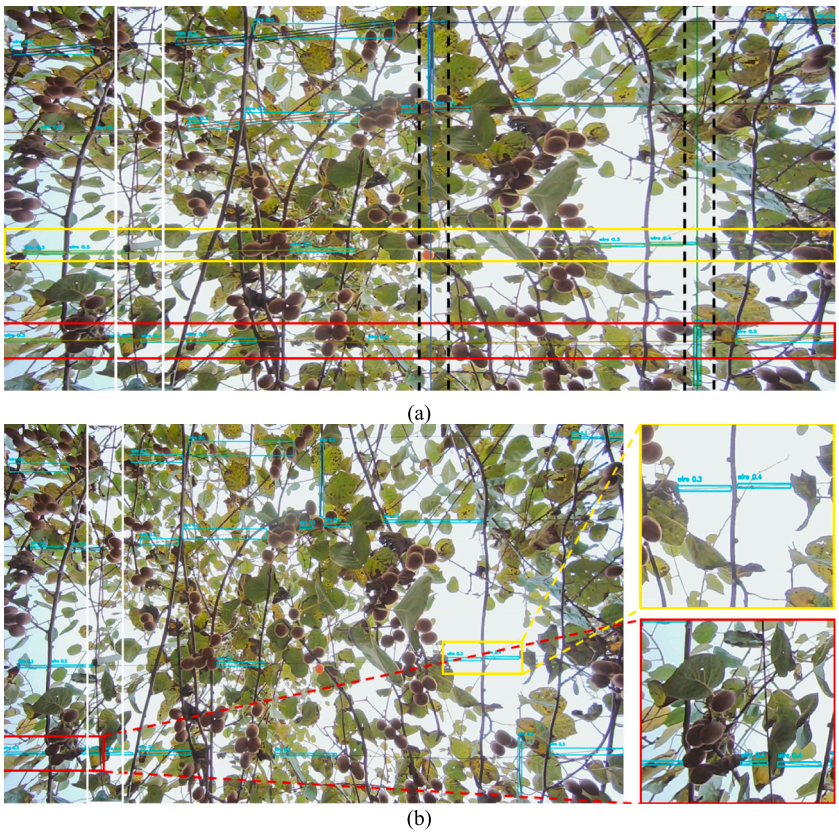


Fig. 13. Example of grid-distributed wire reconstruction using the GFG approach in Orchard-1. The solid red and yellow rectangles in (b) highlight wire pixels predicted by the model under illumination interference and leaf occlusion. The white rectangles indicate the identification or reconstruction results of wires in low-density directions, while the black dashed rectangles in (a) represent incorrect wire reconstructions. (For interpretation of the references to colour in this figure legend, the reader is referred to the web version of this article.)

MR represents the percentage of wires that were missed reconstructed relative to the actual number of wires. In contrast, *IR* indicates the percentage of incorrectly reconstructed wires structures, such as false wire connections, wrong orientations, or reconstructed wires without corresponding ground-truth wires, relative to the actual number of wires. Therefore, *RA* and *MR* are calculated based on the actual visible wires, whereas *IR* reflects errors in the reconstructed output. *IR* is not the complement of *RA*, and *RA*, *MR*, and *IR* do not necessarily sum to 100%. These metrics describe reconstruction quality at the image level rather than the frequency of unsafe robotic motion decisions. The formulations of *RA*, *MR*, and *IR* are given in Eq. (12), Eq. (13), and Eq. (14), respectively. Where, the Correct Number (*CN*), Missed Number (*MN*), Incorrect Number (*IN*) correspond to the numbers of correctly reconstructed wires, missed reconstructed wires, and incorrectly reconstructed wires, respectively, while N_{all} represents the actual number of wires in the testing set.

$$RA = \frac{CN}{N_{all}} \tag{12}$$

$$MR = \frac{MN}{N_{all}} \tag{13}$$

$$IR = \frac{IN}{N_{all}} \tag{14}$$

3. Results and discussion

3.1. Performance of grid wire segmentation

3.1.1. Performance of YOLO11x-seg models with overlap-partitioned dataset

YOLO11x-seg model trained on the overlap-partitioned dataset demonstrated improved robustness and segmentation performance for grid wire detection. To evaluate the effectiveness of the overlap-partitioning strategy, a comparative analysis was performed between a model trained on the original dataset and another trained on the overlap-partitioned dataset. The original dataset was prepared through manual annotation and data augmentation, whereas the overlap-partitioned dataset was generated by partitioning both the original image and their corresponding annotations. Both models were trained using identical hyperparameter settings. As shown in Fig. 10, the model trained on the overlap-partitioned dataset achieved lower training loss values, although it required a longer convergence time compared with the model trained on the original dataset. The reduced and smoother loss curves, together with improved evaluation metrics, indicate that the overlap-partitioned strategy effectively enhances feature learning for thin wire structures and improved the overall robustness and accuracy of wire segmentation in dense canopy environment.

YOLO11x-seg model trained on the overlap-partitioned dataset demonstrated superior performance compared with the model trained on the original dataset. As shown in Table 2, the overlap-partitioned model achieved an *AP* of 10.70% and an *AP*50 of 28.50%, whereas the model trained on the original dataset achieved *AP* and *AP*50 values of 4.70% and 15.00%, respectively. The performance improvement can be primarily attributed to the increased proportion of wire pixels within

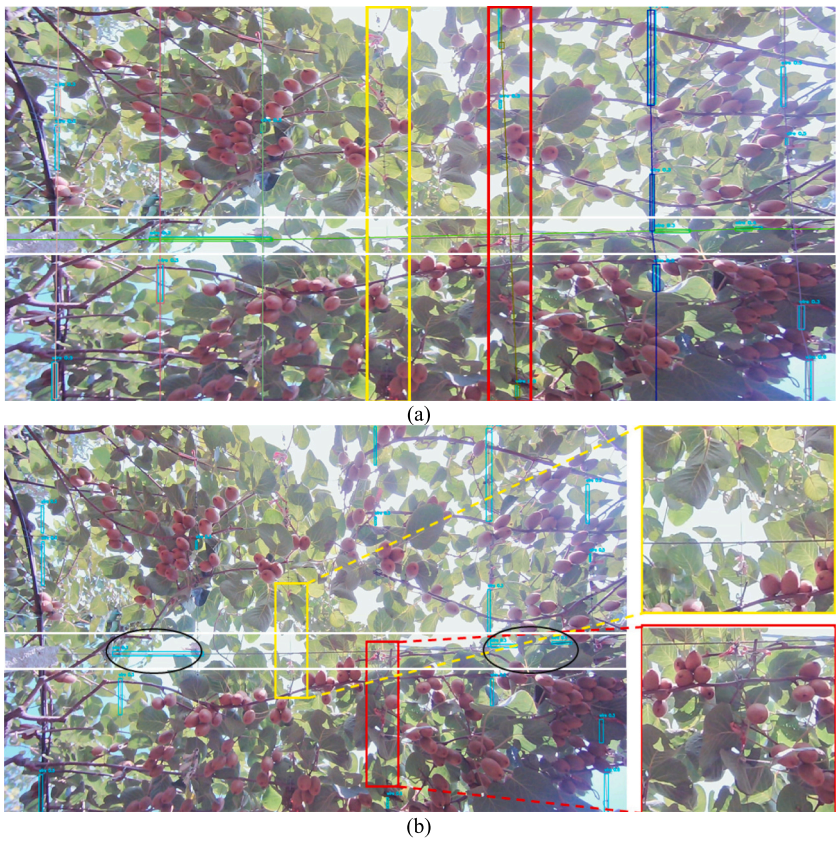


Fig. 14. Example of grid-distributed wire reconstruction using the GFG approach in Orchard-2. The solid red and yellow rectangles in (a) indicate that the model fails to identify wire features under illumination interference and leaf occlusion. The white rectangles represent the identification or reconstruction results of wires in low-density directions, while the black solid circles in (b) denote correctly identified wires. (For interpretation of the references to colour in this figure legend, the reader is referred to the web version of this article.)

the overlap-partitioned dataset, which enhances feature representation and improves the network's learning efficiency [11]. These results demonstrate that the overlap-partitioned strategy significantly improves wire segmentation performance and provides more reliable inputs for the subsequent wire reconstruction process.

3.1.2. Performance of YOLO11x-seg models with IOS on wire segmentation

YOLO11x-seg model integrated with IOS strategy demonstrated enhanced performance in grid wire segmentation. To evaluate segmentation performance on full-resolution canopy images, the YOLO11x-seg model with IOS was compared against a baseline model without IOS, in which the original full images were directly input into the network without overlap-partitioning or stitching post-processing. As shown in Table 3, the YOLO11x-seg model with IOS achieved an *IoU* of 21.19% and a *PA* of 21.00%, corresponding to improvements of 9.54% and 10.00%, respectively, compared with the baseline model without IOS. These results indicate that the IOS strategy effectively enhances segmentation performance by increasing the representation of wire features, enabling more accurate identification of thin grid-distributed wire pixels within dense canopy environments [11].

Segmenting grid-distributed wires within dense kiwifruit canopies is substantially more challenging than segmenting wires arranged along a single direction. Previous studies have reported promising segmentation performance under relatively less complex orchard conditions and have provided valuable methodological insights [11,14,26], however, most of these studies primarily focused on single-direction wire arrangements. In contrast, the present study addresses a significantly more complex grid-structure wire system under dense canopy conditions during harvesting season. The relatively low *IoU* and *PA* values obtained without IOS (Table 3) highlight the difficulty of this task, particularly due to the limited pixel representation of thin wire structures within high-resolution canopy images. By applying the IOS strategy, segmentation performance was substantially improved through increased effective wire pixel representation and enhanced local feature extraction capability. These findings demonstrate that IOS is an effective approach for improving segmentation robustness and accuracy in complex grid-distributed detection scenarios within dense orchard environments.

YOLO11x-seg integrated with the IOS strategy required longer processing time for full-resolution images compared with direct segmentation without IOS. Specifically, overlap partitioning of a complete full-resolution image (2560 × 1440 pixels) required 290.00 ms, whereas model processing of each overlap-partitioned sub-image (1024 × 800 pixels) required 174.80 ms, and stitching the segmented sub-images into a full-resolution image required 117.20 ms. Since each original image was divided into six sub-images, the total processing time for segmenting a full-resolution image using the IOS strategy reached 1456.00 ms. Compared with the wire segmentation results reported by Jiang et al. [11], these findings further highlight the increased difficulty and computational burden of segmenting grid-distributed wires within dense kiwifruit canopies, even when employing IOS strategy with a predefined overlap rate.

These findings suggest that the practical applicability of IOS strategy should be evaluated not only in terms of segmentation performance, but also with respect to computational cost and the influence of segmentation errors on downstream robotic harvesting. Although IOS improves the segmentation of thin grid-distributed wires, practical robotic deployment still requires lightweight segmentation models, parallel sub-image processing, and edge-device optimization to balance segmentation accuracy, inference speed, GPU utilization, and power consumption [34]. In downstream robotic harvesting, missed wire segments may lead

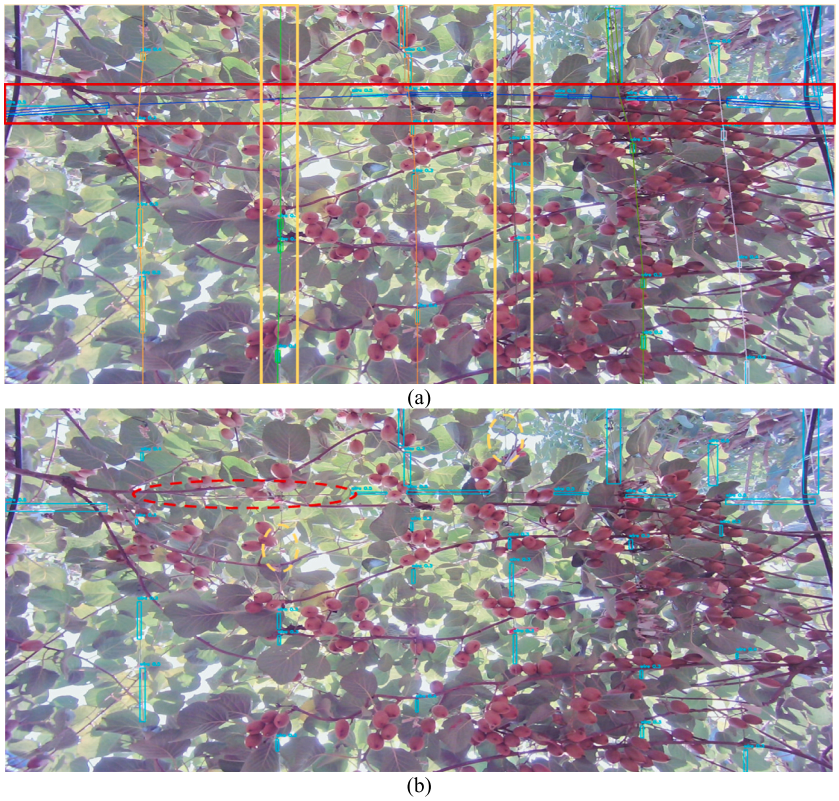


Fig. 15. Examples of grid-distributed wire reconstruction using the GFG approach under moderate illumination conditions. The horizontal red ellipse and vertical yellow dashed ellipse in (b) are not identified due to illumination interference. The red and yellow rectangles in (a) indicate the correct wire reconstructions. (For interpretation of the references to colour in this figure legend, the reader is referred to the web version of this article.)

to incomplete obstacle representation in the reconstructed wire layout, whereas false-positive wire segments may create overly conservative obstacle regions and reduce feasible end-effector approach paths. Although GFG approach can reconnect fragmented, direction-consistent wire segments, it cannot fully compensate for segmentation level failures, such as completely missed wires or non-wire structures incorrectly entering reconstruction stage.

Some incorrect wire segmentations were observed in the test images processed using YOLO11x-seg model integrated with the IOS strategy. As illustrated in Fig. 11a, the wire pixels extracted by the model are highlighted in sky blue, while the corresponding minimum bounding rectangles display wire labels and confidence scores. However, some certain branch structures, manually annotated with solid red rectangles, were incorrectly segmented as wires because of their similar features. In comparison, Fig. 11b presents an example of grid wire recognition and segmentation obtained from the YOLO11x-seg model without IOS. Although fewer wire segments are detected in this case, the identified wires regions exhibit relatively high segmentation accuracy, further demonstrating the superior segmentation performance of YOLO11x-seg in complex orchard environments. Nevertheless, distinguishing thin wires from visually similar branches and canopy structures remains inherently challenging, and such false-positive detections contribute to the relatively low overall segmentation accuracy for grid-distributed wires, even when the IOS strategy is applied.

3.2. Performance of grid wire reconstruction

3.2.1. Performance of grid wire reconstruction based on GFG approach

The proposed GFG approach demonstrated favorable performance for reconstructing grid-distributed wires in dense kiwifruit canopies. Table 4 summarizes the quantitative evaluation results of grid wire reconstruction using the GFG approach. As shown in Table 4, the proposed method achieved a reconstruction accuracy of 78.28%, which is lower than the accuracies reported by Jiang et al. [11] and Song et al. [3], but comparable to the performance by Kok et al. [14]. The reduced reconstruction accuracy can be mainly attributed to the complex and irregular canopy structures, where severe occlusions, fragmented wire segments, and visually similar branches introduce challenges for accurate grouping and continuity estimation. Despite these challenges, the proposed method achieved a relatively low missed reconstruction rate of 4.51%, which remains lower than the value reported by Song et al. [3]. In terms of computational efficiency, the proposed GFG required 487 ms to reconstruct grid wires from the full-resolution images (2560 $\times$ 1440 pixels), whereas the FPEF-based method proposed by Jiang et al. [11] required 730 ms for higher-resolution images (3648 $\times$ 5472 pixels). It should be noted that all comparative metrics discussed here are based on the same indicator definitions and evaluation methods reported in the corresponding cited studies. Overall, these results demonstrate that the proposed GFG approach provides promising feasibility and computational efficiency for grid wire reconstruction in dense orchard environments.

The relatively high *IR* value indicates that incorrect geometric connections, orientation errors, or additional non-existent wire structures were generated during reconstruction. For robotic harvesting, the practical influence of these incorrect reconstructions depends on their proximity to the end-effector approach path and whether they correspond to real obstacles in depth space [14]. Therefore, the *IR* value is an image-level reconstruction error that may introduce false geometric constraints in the reconstructed wire layout, rather than as a direct proportion of unsafe robotic decisions.

The proposed GFG approach is more suitable for reconstructing grid-distributed wires compared to existing methods. Unlike previous studies [3,11,14], the kiwifruit canopy considered in this work contains a curved grid-like distribution of horizontal and vertical wires, where the

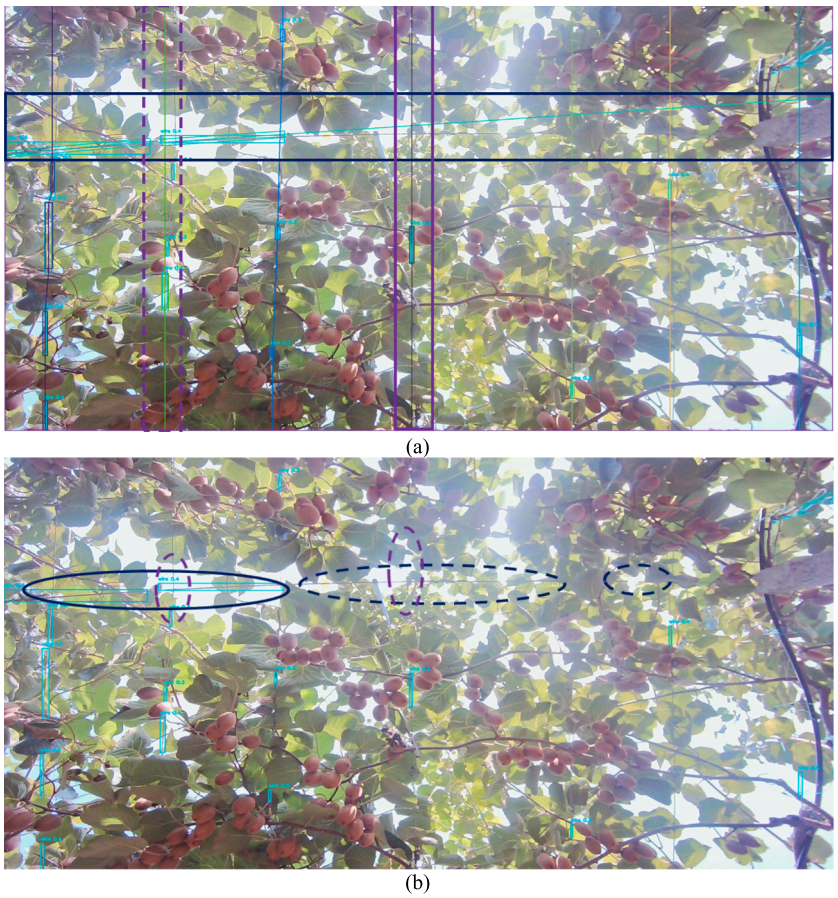


Fig. 16. Examples of grid-distributed wire reconstruction using the GFG approach under strong illumination conditions. The horizontal dark blue solid ellipse obscured by leaves in (b) are successfully identified, whereas other segments in dashed ellipses are completely missed due to strong light. The dark blue and left purple rectangles indicate incorrect wire reconstructions, but the right purple rectangle in (a) are still reconstructed from limited identifications. (For interpretation of the references to colour in this figure legend, the reader is referred to the web version of this article.)

yellow rectangle highlights a representative horizontal wires and the red rectangle indicates a vertical wire (Fig. 12a). This complex spatial configuration introduces substantial reconstruction challenges due to wire curvature, occlusion, and irregular continuity within dense canopy environments. To address these challenges, the proposed GFG approach reconstructs continuous wire structures from fragmented wire segments predicted by YOLO11x-seg through a structured three-stage pipeline. Specifically, Stage-1 performs directional classification to ensure consistent wire grouping, Stage-2 establishes spatial continuity among wire segments within the same groups, and Stage-3 completes the final grid-distributed wire reconstruction.

Reconstructed wire layout provides useful spatial information, but it should not be interpreted as direct end-effector guidance. As shown in Fig. 12b, slight positional deviations may still occur. Thus, the results highlight image-level reconstruction for approximating the spatial arrangement and distribution of grid-distributed wires in dense canopy scenes. For practical robotic harvesting, this geometric reference may support future systems for collision avoidance and fruit approach path planning [14], but it should be further combined with camera-robot calibration, depth perception, conservative safety margins, and closed-loop robotic validation [11]. In contrast, previous studies primarily focused on orchard environments with relatively uniform and linear wire distributions. Consequently, existing reconstruction methods based on PPHT [3] and FPEF [11] are mainly constrained to line-based detection and polynomial fitting strategies commonly used in lane-line reconstruction applications [35,36]. Similarly, the spatial reconstruction approach [14] developed for apple orchards is susceptible to severe occlusions caused by leaves, fruits, and illumination variations in dense kiwifruit canopies, which can hinder complete and continuous reconstruction of grid-distributed wires in T-bar trellis systems. It should be noted that the proposed GFG approach is suitable for structured T-trellis orchard scenes, but it is not intended for direct application to unstructured orchard systems. Further adaptation would be required before applying the method to orchards without regular wire layouts.

3.2.2. *Discussion of grid wire reconstruction in different scenarios*

The performance of grid wire reconstruction under varying canopy conditions warrants further discussion. Figs. 13a and 14a present examples of grid-distributed wire reconstruction using the proposed GFG approach in two different orchards, while Figs. 13b and 14b illustrate the corresponding wire segmentation results obtained from YOLO11x-seg integrated with IOS strategy prior to reconstruction. In these figures, distinct colored lines denote reconstructed wires, whereas rectangles or circles in different colors indicate wire identification and reconstruction results. Due to the extremely thin structure of canopy wires, reliable feature extraction remains challenging for deep learning-based segmentation models. In Orchard-1, several wires highlighted by red and yellow rectangles (Fig. 13b) were affected by illumination variations or partial occlusion. Nevertheless, these wires segments were accurately segmented and reconstructed in Fig. 13a (i.e., Stage-1, Stage-2, and Stage-3 in GFG were implemented). In contrast, Orchard-2 exhibited a denser canopy with more severe wire occlusions, which substantially hindered wire feature extraction and resulted in missed wire segmentation, as seen in red and yellow rectangles (Fig. 14a). Consequently, wires segments that were not successfully identified during segmentation were also absent from the reconstruction results

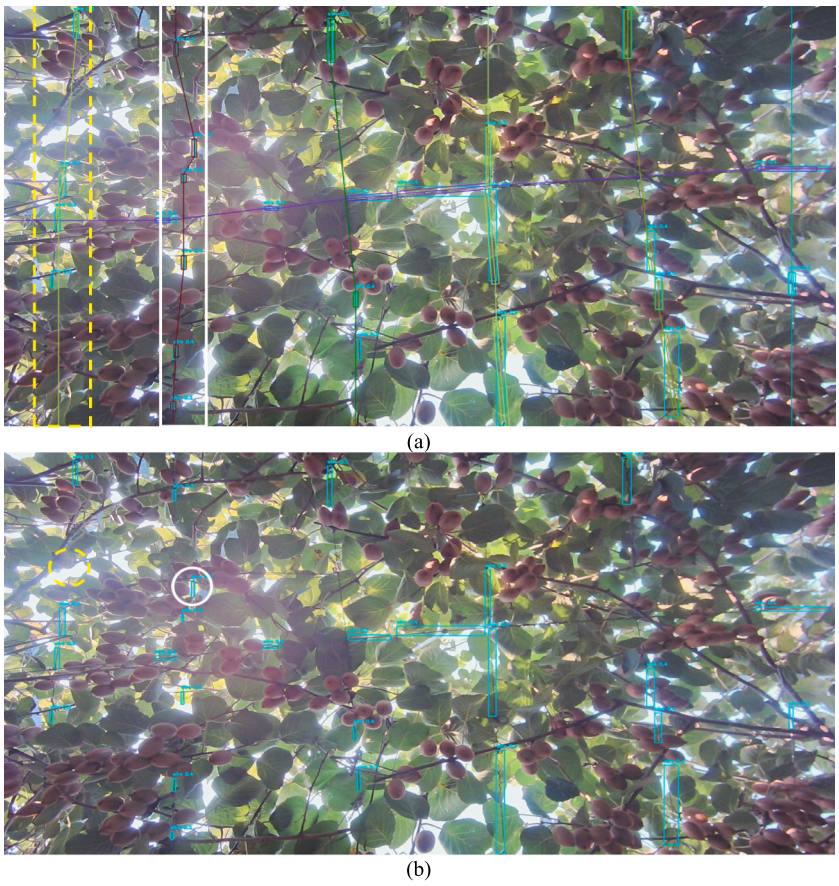


Fig. 17. Examples of grid-distributed wire reconstruction using the GFG approach under weak illumination conditions. The yellow and white ellipses in (b) represent unidentified wires and the branch misidentified as a wire segment. The yellow and white rectangles in (a) indicate the incorrect wire reconstructions. (For interpretation of the references to colour in this figure legend, the reader is referred to the web version of this article.)

shown in Fig. 14a, indicating failure in the initial directional classification stage (Stage-1) of the three-stage processing pipeline. These observations highlight the high sensitivity of wire reconstruction to illumination variations and canopy occlusion.

Wires in less densely populated orientations are typically thicker than those in high- density directions to provide enhanced structural support for canopy management. In Orchard-1, due to the limited representation of wire-like features in the training dataset and the influence of illumination conditions, the model failed to identify the vertical wires inside white rectangle (Fig. 13b), resulting in the missed reconstruction in Fig. 13a (i.e., Stage-1 in GFG was not implemented). Moreover, the black dashed rectangles in Fig. 13a indicate that the branches were misidentified as wires, resulting in incorrect wire reconstructions. In Orchard-2, the horizontal wire marked by the black solid circles was only partially identified (Fig. 14b), while some wires affected by illumination conditions and occluded by leaves were still successfully reconstructed in Fig. 14a (i.e., Stage-1, Stage-2, and Stage-3 in GFG were implemented). Overall, despite a limited number of missed detections and misclassifications in challenging scenarios, the majority of grid-distributed wires were reconstructed with satisfactory accuracy, demonstrating the robustness of proposed approach under complex orchard conditions.

The performance of wire reconstruction under varying illumination conditions is further analyzed and discussed. Since the images collected from Orchard-2 were acquired under sunny conditions with varying illumination conditions, Figs. 15a, 16a, and 17a present the reconstruction results obtained using the proposed GFG approach under moderate, strong, and weak illumination respectively, while Figs. 15b, 16b, and 17b show the corresponding wire segmentation outputs generated from YOLO11x-seg integrated with IOS. Under moderate lighting conditions, certain thin wire segments within horizontal red ellipse and vertical yellow dashed ellipse are not correctly identified due to illumination interference, although other wire segments along the same orientations are successfully identified (Fig. 15b). Despite these partial omissions at the segmentation stage, complete wire structures within the red and yellow rectangles (Fig. 15a) are still reconstructed effectively (i.e., Stage-1, Stage-2, and Stage-3 in GFG were implemented). Therefore, the overall grid-wire reconstruction performance under moderate lighting conditions remains satisfactory.

Wire reconstruction performance varies noticeably under strong and weak illumination conditions across different orchard scenes. Under strong light, some thicker wire segments in horizontal dark blue solid ellipse obscured by leaves are successfully identified, whereas other segments in dashed ellipses are completely missed due to strong light (Fig. 16b), leading to incorrect reconstruction in dark blue and left purple rectangles in Fig. 16a (i.e., Stage-1 in GFG was not implemented), although relatively straight wires in the right purple rectangle are still reconstructed based on limited identifications. Under weak light, reduced illumination and occlusion significantly decrease detectable wire segments in the yellow ellipse, and misidentification of branches in the white ellipse as wires occurs (Fig. 17b), resulting in the incorrect reconstruction of wires within the yellow and white rectangles (i.e., Stage-1 in GFG was not implemented), as seen in Fig. 17a. Based on the above analysis, the wire reconstruction results should be regarded as a qualitative comparison rather than a controlled quantitative evaluation, because illumination intensity was not recorded for each image and lighting varied continuously across canopy scenes. Overall, these results demonstrate that grid-distributed wire reconstruction is highly sensitive

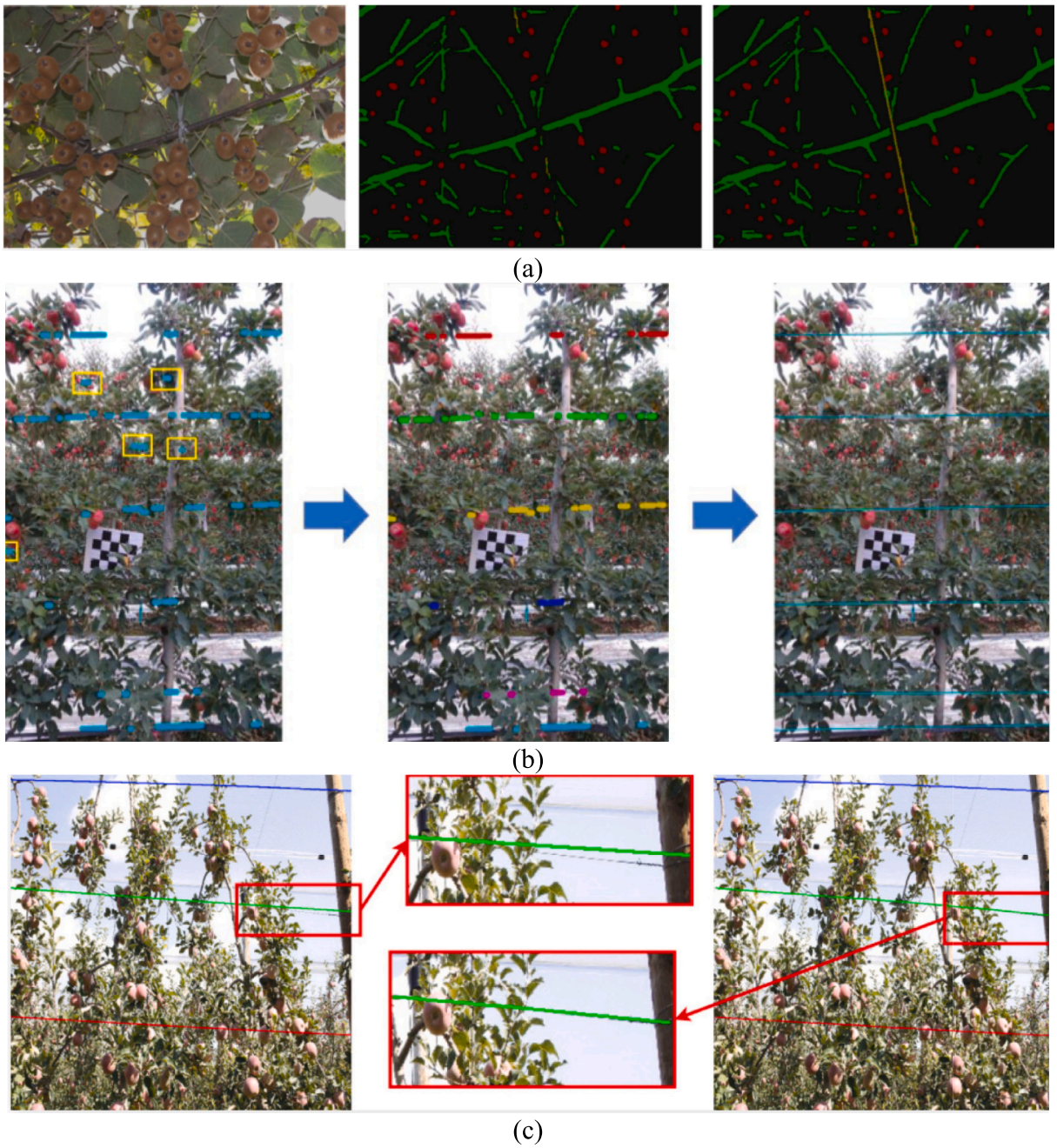


Fig. 18. Visualization of wire reconstruction from previous studies, where the reconstruction methods refer to (a) PPHT [3], (b) FPEF [11], and (c) spatial reconstruction [14], respectively.

to illumination intensity under diverse lighting conditions in different canopy scenarios. Although GFG approach is sensitive to illumination variations and canopy occlusion, it remains applicable across diverse kiwifruit canopy environments. Furthermore, the results indicate that the Stage-1, Stage-2, and Stage-3 of the GFG are closely linked, with Stage-1 playing a fundamental and critical role in grouping grid wire structure.

A review of prior studies reveals notable differences in canopy grid structures compared with those addressed in this work. In kiwifruit orchard, Song et al. [3] focused on close-range images containing one to three wires in a single orientation, with only a few cases involving simple grids of four wires (Fig. 18a). In these settings, wire thickness between low- and high-density directions show minimal variation, and the wires are largely linear with negligible curvature. Such simplified structural characteristics enable reliable wire reconstruction using PPHT-based methods. Similarly, previous studies in apple orchards mainly consider unidirectional wires layouts with uniform thickness (Fig. 18b, c), where reconstruction methods based on feature point fitting [11] or spatial reconstruction [14] perform effectively under well-structured and less occluded conditions. In contrast, the wire configurations in this study exhibit a more complex grid-distributed structure (Fig. 12). To address these challenges the proposed GFG effectively reconstructs complete grid-distributed wires by integrating discrete segmented outputs into continuous representations, where Stage-1 plays a critical role in determining the success of subsequent Stage-2 and Stage-3 operations. Overall, the proposed GFG approach enables robust integration of fragmented wire segments into a complete and continuous grid structure, thereby enhancing the robot's perception of complex canopy environments and supporting safer approach and more accurate robot end-effector navigation for target fruit approach harvesting

operations.

4. Conclusions

This study proposed a novel method for identifying and reconstructing grid-distributed wire in dense kiwifruit canopies to support obstacle awareness for robotic harvesting. YOLO11x-seg model achieved an *AP*50 of 28.50% at an *IoU* threshold of 0.5 on the overlap-partitioned dataset, outperforming the results obtained using the original dataset, indicating that overlap-partitioned training significantly improves feature learning for thin wire structures. Furthermore, the model integrated with IOS achieved an *IoU* of 21.19% and a *PA* of 21.00%, both higher than those without IOS, demonstrating that IOS strategy effectively enhanced wire segmentation performance. These results also confirm that grid-distributed wire segmentation is inherently more challenging than single-direction wire segmentation because of greater structural complexity and occlusion. Additionally, the proposed GFG approach achieved a reconstruction accuracy of 78.28%, with directional classification playing a critical role in grouping grid-wire structures and supporting subsequent reconstruction. Although wire reconstruction remains sensitive to illumination variations and canopy occlusions, GFG showed suitability for reconstructing grid-distributed wire across diverse canopy environments. Overall, these findings illustrate that the proposed GFG approach can effectively reconstruct grid-distributed wire structures in dense T-trellis kiwifruit canopy environments, highlighting the importance of reconstructing non-target support structures for improving orchard scene understanding and providing useful geometric information for future obstacle-aware robotic harvesting.

Future work will integrate robust segmentation models with depth information to achieve more accurate wire localization and safer robotic harvesting. To reduce reliance on fixed horizontal or vertical assumptions, adaptive orientation estimation, depth-plane consistency, and learning-based grouping strategies will be explored to suppress false geometric connections and improve robustness under different trellis structures and wire-curvature patterns. In addition, multi-view and temporal fusion from moving robotic platforms will be investigated to alleviate blur caused by viewpoint changes and partial occlusion, although wires completely hidden by leaves or fruits may still remain unrecoverable from feasible viewpoints beneath the canopy. For practical smart-orchard deployment, the proposed vision framework will be further integrated with agricultural IoT architectures through edge computing, secure data transmission, and efficient storage of high-resolution canopy data, allowing reconstructed wire layouts to support both robotic harvesting and orchard monitoring.

Declaration of generative AI in scientific writing.

The manuscript was not authored with the assistance of artificial intelligence (AI).

The utilization of artificial intelligence (AI)–generated text in an article must be disclosed. During the preparation of this work, the authors used ChatGPT in order to improve the readability and language of the manuscript. After using this tool, the authors reviewed and edited the content as needed and take full responsibility for the content of the published article.

CRediT authorship contribution statement

Xiaojuan Liu: Writing – review & editing, Writing – original draft, Supervision, Methodology, Investigation, Conceptualization. **Bryan Gilbert Murengami:** Writing – review & editing, Methodology, Investigation, Conceptualization. **Qilin Gong:** Writing – review & editing, Methodology, Investigation, Conceptualization. **Xiaoyu Ma:** Writing – review & editing, Methodology, Data curation, Conceptualization. **Rui Li:** Writing – review & editing, Supervision, Methodology, Conceptualization. **Xiancun Zhou:** Writing – review & editing, Investigation, Data curation, Conceptualization. **Bao Zhou:** Writing – review & editing, Investigation, Formal analysis, Conceptualization. **Jinyong Chen:** Writing – review & editing, Investigation, Conceptualization. **Ramesh Kumar Sahni:** Writing – review & editing, Investigation, Conceptualization. **Yaqoob Majeed:** Writing – review & editing, Methodology, Investigation. **Spyros Fountas:** Writing – review & editing, Supervision, Methodology. **Longsheng Fu:** Writing – review & editing, Supervision, Methodology, Conceptualization.

Ethics statement

Not applicable: This manuscript does not include human or animal research.

If this manuscript involves research on animals or humans, it is imperative to disclose all approval details.

Declaration of competing interest

The authors declare that they have no known competing financial interests or personal relationships that could have appeared to influence the work reported in this paper.

Acknowledgements

This work was partially supported by the National Natural Science Foundation of China (32501786, 32371999); Chinese Universities Scientific Fund (2452026021); National Foreign Expert Project, Ministry of Human Resources and Social Security, China (H20240238, Y20240046); Key Research and Development Program of Shaanxi, China (2024PT-ZCK-27, 2024NC-YBXM-195); Central Public-interest Scientific Institution Basal Research Fund, China (1610192023105); National Key Research and Development Program (2022YFD1600700).

Data availability

Data is available at https://github.com/Smart-Ag/Kiwifruit_wire_identification_images.

References

[1] Fu L, Tola E, Al-Mallahi A, Li R, Cui Y. A novel image processing algorithm to separate linearly clustered kiwifruits. Biosyst Eng 2019;183:184–95. https://doi.org/10.1016/j.biosystemseng.2019.04.024.

[2] Fu L, Feng Y, Wu J, Liu Z, Gao F, Majeed Y, et al. Fast and accurate detection of kiwifruit in orchard using improved YOLOv3-tiny model. Precis Agric 2020;22:754–76. https://doi.org/10.1007/s11119-020-09754-y.

[3] Song Z, Zhou Z, Wang W, Gao F, Fu L, Li R, et al. Canopy segmentation and wire reconstruction for kiwifruit robotic harvesting. Comput Electron Agric 2021;181:105933. https://doi.org/10.1016/j.compag.2020.105933.

[4] Fu L, Gao F, Wu J, Li R, Karkee M, Zhang Q. Application of consumer RGB-D cameras for fruit detection and localization in field: a critical review. Comput Electron Agric 2020;177:105687. https://doi.org/10.1016/j.compag.2020.105687.

[5] Kumar D, Pawar P, Meesala M, Pareek P, Addula S, Shwetha K. Smart agriculture in the era of Big Data: IoT-assisted pest forecasting and resource optimization for sustainable farming. ICIICS (International Conference on Integrated Intelligence and Communication Systems). 2024. p. 1–8. https://doi.org/10.1109/ICIICS63763.2024.10860125.

[6] Jing X, Jiang H, Niu S, Zhang H, Gilbert M, Wu Z, et al. End-to-end stereo matching network with two-stage partition filtering for full-resolution depth estimation and precise localization of kiwifruit for robotic harvesting. Comput Electron Agric 2024;225:109333. https://doi.org/10.1016/j.compag.2024.109333.

[7] Liu X, Jing X, Jiang H, Younas S, Wei R, Dang H, et al. Performance evaluation of newly released cameras for fruit detection and localization in complex kiwifruit orchard environments. J Field Robot 2024;41(4):881–94. https://doi.org/10.1002/rob.22297.

[8] Williams H, Jones M, Nejati M, Seabright M, Bell J, Penhall N, et al. Robotic kiwifruit harvesting using machine vision, convolutional neural networks, and robotic arms. Biosyst Eng 2019;181:140–56. https://doi.org/10.1016/j.biosystemseng.2019.03.007.

[9] Fu L, Majeed Y, Zhang X, Karkee M. Faster R-CNN-based apple detection in dense-foliage fruiting-wall trees using RGB and depth features for robotic harvesting.

Biosyst Eng 2020;197:245–56. https://doi.org/10.1016/j.biosystemseng.2020.07.007.
[10] Suo R, Gao F, Zhou Z, Fu L, Song Z, Dhupia J, et al. Improved multi-classes kiwifruit detection in orchard to avoid collisions during robotic picking. Comput Electron Agric 2021;182:106052. https://doi.org/10.1016/j.compag.2021.106052.
[11] Jiang H, Sun X, Fang W, Fu L, Li R, Cheein F, et al. Thin wire segmentation and reconstruction based on a novel image overlap-partitioning and stitching algorithm in apple fruiting wall architecture for robotic picking. Comput Electron Agric 2023;209:107840. https://doi.org/10.1016/j.compag.2023.107840.
[12] Gao F, Fu L, Zhang X, Majeed Y, Li R, Karkee M, et al. Multi-class fruit-on-plant detection for apple in SNAP system using faster R-CNN. Comput Electron Agric 2020;176:105634. https://doi.org/10.1016/j.compag.2020.105634.
[13] Williams H, Ting C, Nejati M, Jones M, Penhall N, Lim J, et al. Improvements to and large-scale evaluation of a robotic kiwifruit harvester. J Field Robot 2020;37(2):187–201. https://doi.org/10.1002/rob.21890.
[14] Kok E, Liu T, Chen C. Trellis wire reconstruction by line anchor-based detection with vertical stereo vision. Comput Electron Agric 2025;231:109948. https://doi.org/10.1016/j.compag.2025.109948.
[15] Badgujar C, Poulose A, Gan H. Agricultural object detection with you only look once (YOLO) algorithm: a bibliometric and systematic literature review. Comput Electron Agric 2024;223:109090. https://doi.org/10.1016/j.compag.2024.109090.
[16] Li H, Gu Z, He D, Wang X, Huang J, Mo Y, et al. A lightweight improved YOLOv5s model and its deployment for detecting pitaya fruits in daytime and nighttime light-supplement environments. Comput Electron Agric 2024;220:108876. https://doi.org/10.1016/j.compag.2024.108876.
[17] Yang R, Yuan D, Zhao M, Zhao Z, Zhang L, Fan Y, et al. Camellia oleifera tree detection and counting based on UAV RGB image and YOLOv8. Agriculture 2024;14(10):1789. https://doi.org/10.3390/agriculture14101789.
[18] Mao W, He L, Xia M, Jiang H, Li R, Sahni K, et al. A novel method to detect stem and fruit dynamically for apricot posture estimation and adjustment. Inf Process Agric 2025;12:358–69. https://doi.org/10.1016/j.inpa.2024.12.001.
[19] Fu Y, Wang Z, Zheng H, Yin X, Fu W, Gu Y. Integrated detection of coconut clusters and oriented leaves using improved YOLOv8n-obb for robotic harvesting. Comput Electron Agric 2025;231:109979. https://doi.org/10.1016/j.compag.2025.109979.
[20] Li P, Chen J, Chen Q, Huang L, Jiang Z, Hua W, et al. Detection and picking point localization of grape bunches and stems based on oriented bounding box. Comput Electron Agric 2025;233:110168. https://doi.org/10.1016/j.compag.2025.110168.
[21] Ma B, Sun L, Mu H, Ren Z, Kang G, Liu R, et al. MH-YOLO: multiple heterogeneous YOLO for apple orchard pest detection. Inf Process Agric 2025. https://doi.org/10.1016/j.inpa.2025.08.001.
[22] Zhang X, Zhang G, Wang J, Yang J, Ge Q, Zhao R, et al. Efficient instance segmentation for strawberry in greenhouses using YOLOv8n-MCP on edge devices. Inf Process Agric 2025. https://doi.org/10.1016/j.inpa.2025.07.001.
[23] Qiao C, Li K, Zhu X, Jing J, Gao W, Zhang L. Detection of cucumber downy mildew spores based on improved YOLOv5s. Inf Process Agric 2025;12:179–94. https://doi.org/10.1016/j.inpa.2024.05.002.
[24] Liu B, Zhang Y, Wang J, Luo L, Lu Q, Wei H, et al. An improved lightweight network based on deep learning for grape recognition in unstructured environments. Inf Process Agric 2024;11:202–16. https://doi.org/10.1016/j.inpa.2023.02.003.
[25] Sapko R, Meng Z, Churuvija M, Du X, Ma Z, Karkee M. Comprehensive performance evaluation of YOLO11, YOLOv10, YOLOv9 and YOLOv8 on detecting and counting fruitlet in complex orchard environments. arXiv 2024;2407:12040. https://doi.org/10.48550/arXiv.2407.12040.
[26] Majeed Y, Zhang J, Zhang X, Fu L, Karkee M, Zhang Q. Deep learning based segmentation for automated training of apple trees on trellis wires. Comput Electron Agric 2020;170:105277. https://doi.org/10.1016/j.compag.2020.105277.
[27] Gao C, He L, Ding Y, Murengami B, Chen J, Zhou C, et al. A novel multinozzle targeting pollination robot for clustered kiwifruit flowers based on air-liquid dual-flow spraying. J Field Robot 2025;42:2136–50. https://doi.org/10.1002/rob.22499.
[28] Mu L, Liu H, Cui Y, Fu L, Gejima Y. Mechanized technologies for scaffolding cultivation in the kiwifruit industry: a review. Inf Process Agric 2018;5(4):401–10. https://doi.org/10.1016/j.inpa.2018.07.005.
[29] Wada K. Labelme: Image polygonal annotation with python. 2018. https://github.com/wkentaro/labelme.
[30] Wu Z, Sun X, Jiang H, Mao W, Li R, Andriyanov N, et al. NDMFCS: an automatic fruit counting system in modern apple orchard using abatement of abnormal fruit detection. Comput Electron Agric 2023;211:108036. https://doi.org/10.1016/j.compag.2023.108036.
[31] Zhang M, Liang H, Wang Z, Wang L, Huang C, Luo X. Damaged apple detection with a hybrid YOLOv3 algorithm. Inf Process Agric 2024;11(2):163–71. https://doi.org/10.1016/j.inpa.2022.12.001.
[32] Jocher G, Chaurasia A, Qiu J. Ultralytics YOLO11. San Francisco, CA, USA: GitHub; 2024. https://github.com/ultralytics/ultralytics.
[33] Wang Z, Su Y, Kang F, Wang L, Lin Y, Wu Q, et al. PC-YOLO11s: a lightweight and effective feature extraction method for small target image detection. Sensors (Basel, Switzerland) 2025;25(2):348. https://doi.org/10.3390/s25020348.
[34] Bakirci M. Performance evaluation of low-power and lightweight object detectors for real-time monitoring in resource-constrained drone systems. Eng Appl Artif Intel 2025;159:111775. https://doi.org/10.1016/j.engappai.2025.111775.
[35] Marzougui M, Alasiry A, Kortli Y, Baili J. A lane tracking method based on progressive probabilistic hough transform. IEEE Access 2020;8:84893–905. https://doi.org/10.1109/ACCESS.2020.2991930.
[36] Bhusal S, Bhattarai U, Karkee M. Trellis wire detection for obstacle avoidance in apple orchards. IFAC-PapersOnLine 2022;55(32):72–7. https://doi.org/10.1016/j.ifacol.2022.11.117.



Xiaojuan Liu, Doctoral Candidate (College of Mechanical and Electronic Engineering, Northwest A&F University, Electrification and Automation of Agriculture), Master Degree from Gansu Agricultural University, Research on Intelligent Information Perception of Agriculture, and Email: wendaoxiao@nwafu.edu.cn.



Bryan Gilbert Murengami, Doctoral Candidate (College of Mechanical and Electronic Engineering, Northwest A&F University, Electrification and Automation of Agriculture), Master Degree from Fujian Agriculture and Forestry University, Research on Intelligent Information Perception of Agriculture, and Email: bryangilbert006@nwafu.edu.cn.



Qilin Gong, Master Candidate (College of Mechanical and Electronic Engineering, Northwest A&F University, Electrification and Automation of Agriculture), Bachelor Degree from Northwest A&F University, Research on Intelligent Information Perception of Agriculture, and Email: code@nwafu.edu.cn.



Xiaoyu Ma, Master Candidate (College of Mechanical and Electronic Engineering, Northwest A&F University, Electrification and Automation of Agriculture), Bachelor Degree from Shanxi Agricultural University, Research on Intelligent Information Perception of Agriculture, and Email: maxiaoyu@nwafu.edu.cn.



Rui Li, Senior Laboratory Technician, Northwest A&F University, Doctoral Degree (Northwest A&F University, College of Mechanical and Electronic Engineering, Agricultural Mechanization Engineering), Research on Processing and Storage of Agricultural Products, and Email: ruili1216@nwafu.edu.cn.



Ramesh Kumar Sahni, Scientist, Agricultural Mechanization Division, ICAR-Central Institute of Agricultural Engineering, Doctoral Degree (Washington State University, Biological and Agricultural Engineering), Research on Precision Agriculture, Farm Mechanization, Sensor systems, Energy-saving Agricultural Machinery, and Email: ramesh.sahni@icar.gov.in.



Xiancun Zhou, Professor, West Anhui University, School of Electronic Information and Artificial Intelligence, Master Degree (Hefei University of Technology, Computer Application Technology), Research on Intelligent Perception and Detection in Agriculture, Intelligent Processing of Agricultural Data, and Email: zhouxcun@wxc.edu.cn.



Yaqoob Majeed, Assistant Professor, Department of Electrical Engineering and Computer Science, University of Wyoming, Doctoral Degree (Washington State University, Biological and Agricultural Engineering), Research on Agricultural Robots, Precision Agriculture, Digital Agriculture, Machine Vision, and Deep Learning, and Email: yaqoob.majeed@ag.tamu.edu.



Bao Zhou, Research Assistant, West Anhui University, School of Electronic Information and Artificial Intelligence, Doctoral Degree (Kunming University of Science and Technology, Faculty of Land Resources Engineering), Research on Intelligent Information Perception of Agriculture, and Email: 03000085@wxc.edu.cn.



Spyros Fountas, Assistant Professor, Agricultural University of Athens, Department of Natural Resources Management and Agricultural Engineering, Doctoral Degree (Copenhagen University, Faculty of Life Sciences), Research on Mechanized and Intelligent Pollination, and Email: sfountas@aua.gr.



Jinyong Chen, Research Fellow, Chinese Academy of Agricultural Sciences, Zhengzhou Fruit Research Institute, Bachelor Degree from Chinese Academy of Agricultural Sciences, Pomology, Fruit cultivation and physiology. Research on High-quality, High-yield and Efficient Cultivation Techniques for Fruit Trees, and Email: chenjinyong@caas.cn.



Longsheng Fu, Professor, College of Mechanical and Electronic Engineering, Northwest A&F University, Key Laboratory of Agricultural Internet of Things, Ministry of Agriculture and Rural Affairs, Doctoral Degree (Hokkaido University, Science of Environmental Resources), Research on Smart Agricultural Technology and Equipment, Agricultural Robotics, and Email: fulsh@nwafu.edu.cn.